DISSERTATIONS IN
FORESTRY AND
NATURAL SCIENCES

Henri Partanen

Modeling and measurement of partial spatial coherence

Publications of the University of Eastern Finland
Dissertations in Forestry and Natural Sciences No 209

UNIVERSITY OF
EASTERN FINLAND

HENRI PARTANEN

Modeling and measurement of partial spatial coherence

Publications of the University of Eastern Finland
Dissertations in Forestry and Natural Sciences
No 209

Academic Dissertation
To be presented by permission of the Faculty of Science and Forestry for public examination in the Auditorium M101 in Metria Building at the University of Eastern Finland, Joensuu, on December 18, 2015, at 12 o'clock noon.

Department of Physics and Mathematics

Grano Oy
Jyväskylä, 2015
Editors: Prof. Pertti Pasanen, Prof. Kai Peiponen,
Prof. Pekka Kilpeläinen, Prof. Matti Vornanen

Distribution:
University of Eastern Finland Library / Sales of publications
julkaisumyynti@uef.fi
http://www.uef.fi/kirjasto

ISBN: 978-952-61-1534-4 (printed)
ISSNL: 1798-5668
ISSN: 1798-5668
ISBN: 978-952-61-1535-1 (pdf)
ISSNL: 1798-5668
ISSN: 1798-5676

Author's address:
University of Eastern Finland
Department of Physics and Mathematics
P. O. Box 111
80101 JOENSUU
FINLAND
email: henri.partanen@uef.fi
alt. email: partanen.h@gmail.com

Supervisors:
Professor Jari Turunen, Dr.Tech.
University of Eastern Finland
Department of Physics and Mathematics
P. O. Box 111
80101 JOENSUU
FINLAND
email: jari.turunen@uef.fi

Associate Professor Jani Tervo, Ph.D.
University of Eastern Finland
Department of Physics and Mathematics
P. O. Box 111
80101 JOENSUU
FINLAND
email: jani.tervo@gmail.com

Reviewers:
Professor José J. Gil, Ph.D.
Universidad de Zaragoza
Facultad de Educación
San Juan Bosco 7
50009 ZARAGOZA
SPAIN
email: ppgil@unizar.es

Associate Professor Juha Toivonen, Dr.Tech.
Tampere University of Techonology
Department of Physics
P. O. Box 692
33101 TAMPERE
FINLAND
email: juha.toivonen@tut.fi

Opponent:
Associate Professor Sergei Popov, Dr.Tech.
Royal Institute of Technology (KTH)
Optics and Photonics Division
Electrum 229
164 40 KISTA
SWEDEN
email: sergeip@kth.se

ABSTRACT

This thesis contains studies on various aspects of partial spatial coherence of light. It includes purely theoretical considerations, numerical simulations on partially coherent beam propagation, construction and use of novel coherence measurement equipment, and experimental results on characterization of light fields emitted by real light sources. In the theoretical studies, the coupling of partially coherent light into planar waveguides is investigated by means of a coherent-mode decomposition of the incident field. Several types of coherent-field representations are applied also to beams radiated by broad-area laser diodes, which are used as practical examples of spatially partially coherent light sources. Interferometric setups are constructed both for coherence measurement and for the construction of interesting types of partially coherent beams of light. The coherence functions of the considered light sources are meandered by a novel realization of the classical Young's double pinhole experiment based on digital micromirror devises. The acquired data is used to simulate the beam propagation with much higher accuracy than before.

Universal Decimal Classification: 531.715, 535.3, 621.372.8, 621.375.826, 681.7.069.24
INSPEC Thesaurus: optics; light; light coherence; light propagation; simulation; modelling; optical variables measurement; light interferometry; light interferometers; micromirrors; semiconductor lasers; optical planar waveguides
Yleinen suomalainen asiasanasto: optiikka; valo; koherenssi; laserit; lasersäteily; simulointi; mallintaminen; mittaus

Preface

I want to thank my supervisors Prof. Jari Turunen and Dr. Jani Tervo for their great help and patience with me, without you this work would not have been possible. You introduced me into the world of coherence.

For financial support I am grateful to Tekniikan edistämissäätiö for a grant to finish the writing of this thesis. I am grateful to the former and present heads of the Department of Physics and Mathematics Pasi Vahimaa, Markku Kuittinen, Seppo Honkanen and Timo Jääskeläinen, for the opportunity to work in the university. Thank you Pertti Pääkkönen and Tommi Itkonen for helping me to build and use my laboratory setups and other practical things.

During my studies I was able to work couple of months in Germany, thank you Prof. Frank Wyrowski and Prof. Wolfgang Osten for inviting me to these research visits to Jena and Stuttgart, and for all the valuable knowledge shared over Europe. Also thank you Olga Baladron Zorita, Christian Hellmann, Site Zhang, Daniel Asoubar, Sandy Peterhänsel, Christof Pruss, and all other who helped and kept me company during these visits.

All the colleges and office roommates, thank you very much Markus, Joonas, Najnin, Manisha, Subhajit, Rahul, Balu, Kimmo and all others for good time in and outside of the university.

Thank you Sanna for being on my side during the good and bad times. My deepest gratitude for my mother, you are the strongest and most loving person I know, and my father, who did not see me finish this work, you were the best dad in the world. This is for you.

Joensuu December 2, 2015 *Henri Partanen*

LIST OF PUBLICATIONS

This thesis consists of the present review of the author's work in the field of optical partial coherence and the following selection of the author's publications:

I H. Partanen, J. Tervo, and J. Turunen, "Spatial coherence of broad-area laser diodes," *Appl. Opt.* **52,** 3221–3228 (2013).

II H. Partanen, J. Turunen, and J. Tervo, "Coherence measurement with digital micromirror device," *Opt. Lett.* **39,** 1034–1037 (2014).

III H. Partanen, N. Sharmin, J. Tervo, and J. Turunen, "Specular and antispecular light beams," *Opt. Exp.* **23,** 28718–28727 (2015).

IV H. Partanen, J. Tervo, and J. Turunen, "Coupling of spatially partially coherent beams into planar waveguides," *Opt. Exp.* **23,** 7879–7893 (2015).

Throughout the overview, these papers will be referred to by Roman numerals.

AUTHOR'S CONTRIBUTION

The publications selected in this dissertation are original research papers in the field of optical coherence theory. All papers are results of group work. The author developed the ideas that lead to the publications in collaboration with the co-authors. He has planned and constructed the experimental setups used in all papers, carried out nearly all of the experiments and numerical simulations, and analyzed all the experimental results reported in the papers. He has also participated actively in the writing of each manuscript.

LIST OF ABBREVIATIONS

The following abbreviations are used in this thesis:

ACF Angular correlation function

BALD Broad-area laser diode

CSD Cross spectral density function

DMD Digital micromirror device

GSM Gaussian Schell model

LED Light-emitting diode

VCSEL Vertical-cavity surface-emitting laser

WFI Wavefront folding interferometer

Contents

1 Introduction

Light emitted by natural sources, such as the sun and other stars, forest fires, or fluorescent creatures lurking in deep oceans, is nearly spatially incoherent. In simple terms, this means that if we apply a two-pinhole mask to isolate two small spatially separated areas of the field emitted by the source and let the radiation from the pinholes propagate further, the observed intensity distribution is essentially the sum of the intensity distributions seen when only one of the pinholes is open. Several man-made light sources, such as lasers, exhibit rather different behavior: if we again sample the field at two spatially separated points and let the resulting fields overlap, interference fringes of high contrast are observed. In this case the field radiated by the source can be characterized as being highly spatially coherent. However, there are many light sources with spatial coherence properties between these two extremes. Such partially spatially coherent light sources produce fringes with reduced contrast in the two-pinhole experiment.

Optical coherence theory provides the methodology to deal with all kinds of light sources referred to above [1–3]. In particular, it allows one to define quantitatively concepts such as the degree of spatial coherence, which specifies how well light fields emanating from the two pinholes can interfere. This theory is of central importance in optics since the effects of the state of spatial coherence of light extend far beyond the two-pinhole experiment. With spatially coherent laser light we can easily see many kinds of interference patterns, including speckle patterns, even when we try to use laser light for even illumination [4, 5]. On the other hand, with thermal light, it is very difficult to see any kind of interference unless the pinholes are spaced within a wavelength-scale distance apart. In the absence of coherent light sources, proving the wave nature of the light was difficult two hundred years ago [6–8]. The visibility of the interference fringes is indeed the traditional definition for

the degree of spatial coherence of light [9], and will be used in this thesis as the basis of our measurement setups.

The degree of coherence is not just a single number, but it depends on the measurement coordinates (pinhole positions). Normally, when the measurement points get further away from the each other, the degree of coherence decreases. On the other hand, when the points approach each other, the degree of coherence goes to unity. However, such qualitative considerations are not sufficient to describe most partially coherent sources, since spatial coherence generally depends also on the absolute positions of the pinholes. To fully model partially coherent light it is, first of all, necessary to quantify the concept of partial coherence, to which end optical coherence theory provides the means. Generally, in this theory, partially coherent fields are described by correlation functions that characterize the nature of partially coherent light in statistical terms. Such correlation function depend, in addition to the spatial coordinates, also on frequency or time. Further, to be exact, the state of polarization of the vectorial light field must be taken into account.

Partial spatial coherence of light implies major numerical modeling problems. The propagation of fully coherent light emitted by a planar source can be treated by two-dimensional integrals, but for partially coherent light the corresponding propagation integrals become four-dimensional. Likewise, the measurement of the optical properties of partially coherent light is a hugely more complicated task than the characterization of a fully spatially coherent field. Treating these problems is the central theme of the present thesis. On the theoretical side, the backbone of the work is the representation of partially coherent light as superpositions of fully coherent modal subfields. The demanding task is to find them. The modes may, for example, correspond to resonator modes of the laser, and we may simulate them, if we know the resonator properties. However, real sources often have imperfections and the shape of the modes may differ considerably from predictions of simple models. Therefore we may have to measure the coherence function

and solve the modes from it. In this thesis we introduce some measurement systems to do this, and discuss how light can be modeled efficiently.

This thesis is organized as follows. In Chapter 2 we introduce the basic concepts of partial spatial coherence. In Chapter 3 we introduce the Gaussian Schell-model source as a simple example of spatially partially coherent sources, and describe how such a source can be modeled numerically using different modal methods. In Chapter 4 we consider real non-ideal light sources and methods to measure their coherence properties, concentrating in particular on broad-area laser diodes. In Chapter 5 we discuss analytical and numerical methods to propagate light in free space and to couple light fields into planar waveguides. Finally, in Chapter 6, some conclusions are drawn and certain possible future directions of the research are outlined.

2 Partial spatial coherence

In this Chapter we define the basic concepts needed to describe the spatial coherence properties of light. We begin by defining the fundamental correlation function of stationary fields in the space-frequency domain, namely the cross spectral density function (CSD), which describes field correlations between two spatial position at a given frequency. Then representations of the CSD by means of superpositions of fully coherent modes are described.

2.1 CROSS-SPECTRAL DENSITY FUNCTION

Restricting the discussion to scalar theory of light, we consider a single component $E(\boldsymbol{r},t)$ of the electric field at position $\boldsymbol{r}=(\boldsymbol{\rho},z)=(x,y,z)$ and time t. In many circumstances it is more convenient to consider the field in the frequency domain. To this end we will use the complex analytic signal representation [1]

$$E(\boldsymbol{r},t)=\int_0^\infty E(\boldsymbol{r},\omega)\exp\left(-\mathrm{i}\omega t\right)\,\mathrm{d}\omega, \tag{2.1}$$

where

$$E(\boldsymbol{r},\omega)=\frac{1}{2\pi}\int_{-\infty}^{\infty}E(\boldsymbol{r},t)\exp\left(\mathrm{i}\omega t\right)\,\mathrm{d}t \tag{2.2}$$

is the electric field at position $\boldsymbol{r}$ and frequency ω. For partially coherent light the electric field fluctuates more or less randomly between two spatial coordinates and two frequencies or instants of time. A statistical description of the field is then appropriate and we may define its correlation properties in the space-frequency domain by introducing a two-frequency CSD

$$W(\boldsymbol{r}_1,\boldsymbol{r}_2,\omega_1,\omega_2)=\langle E^*(\boldsymbol{r}_1,\omega_1)E(\boldsymbol{r}_2,\omega_2)\rangle \tag{2.3}$$

where the sharp brackets denote an ensemble average

$$\langle E^*(\boldsymbol{r}_1,\omega_1)E(\boldsymbol{r}_2,\omega_2)\rangle=\lim_{n=\infty}\frac{1}{N}\sum_{n=1}^{N}E_n^*(\boldsymbol{r}_1,\omega_1)E_n(\boldsymbol{r}_2,\omega_2) \tag{2.4}$$

over a set of individual field realizations $E_n(\boldsymbol{r}, \omega)$, which may be e.g. individual pulses in pulse trains generated by mode-locked lasers or supercontinuum sources.

Let us assume that the light field is stationary, i.e., its space-time correlation properties do not depend on the origin of time but only on the time difference $t_2 - t_1$. In this case different spectral components of the field become mutually uncorrelated [1] and the the two-frequency CSD takes the form

$$W(\boldsymbol{r}_1, \boldsymbol{r}_2, \omega_1, \omega_2) = W(\boldsymbol{r}_1, \boldsymbol{r}_2, \omega_1)\delta(\omega_1 - \omega_2), \tag{2.5}$$

where the CSD describing a stationary field,

$$W(\boldsymbol{r}_1, \boldsymbol{r}_2, \omega) = \langle E^*(\boldsymbol{r}_1, \omega)E(\boldsymbol{r}_2, \omega)\rangle, \tag{2.6}$$

depends spectrally only on a single (absolute) frequency ω. Now the spectral density (intensity of the field at position $\boldsymbol{r}$ and frequency ω) is defined as

$$S(\boldsymbol{r}, \omega) = W(\boldsymbol{r}, \boldsymbol{r}, \omega) = \langle |E(\boldsymbol{r}, \omega)|^2 \rangle. \tag{2.7}$$

Furthermore, we may also introduce a normalized form of the CSD,

$$\mu(\boldsymbol{r}_1, \boldsymbol{r}_2, \omega) = \frac{W(\boldsymbol{r}_1, \boldsymbol{r}_2, \omega)}{[S(\boldsymbol{r}_1, \omega)S(\boldsymbol{r}_2, \omega)]^{1/2}}, \tag{2.8}$$

known as the complex degree of spectral coherence. This complex-valued function satisfies the inequalities $|\mu(\boldsymbol{r}_1, \boldsymbol{r}_2, \omega)| \leq 1$, where the upper bound means complete spatial coherence and the lower bound indicates full incoherence of the field at frequency ω.

In this thesis we will deal mainly with quasimonochromatic fields, which have a narrow spectral bandwidth $\Delta\omega$ around a given center frequency ω_0 of the spectrum. In this case the dependence of the CSD on ω is typically insignificant and we therefore leave it implicit from now on for brevity of notation.

All genuine cross-spectral functions have to be nonnegative definite kernels, which means they have to obey (at any transverse plane $z =$ constant) the condition [10, 11]

$$Q(f) = \iint_{-\infty}^{\infty} W(\boldsymbol{\rho}_1, \boldsymbol{\rho}_2) f^*(\boldsymbol{\rho}_1) f(\boldsymbol{\rho}_2)\, \mathrm{d}^2\rho_1\, \mathrm{d}^2\rho_2 \geq 0, \tag{2.9}$$

for any choice of the function $f(\boldsymbol{\rho})$. Also, for all CSD functions, the following inequality holds:

$$|W(\boldsymbol{\rho}_1, \boldsymbol{\rho}_2)|^2 \leq W(\boldsymbol{\rho}_1, \boldsymbol{\rho}_1) W(\boldsymbol{\rho}_2, \boldsymbol{\rho}_2) = S(\boldsymbol{\rho}_1) S(\boldsymbol{\rho}_2). \tag{2.10}$$

Violating these conditions may lead to clearly non-physical results, such as negative intensities in some positions. Later we see how measurement errors may lead to such a situation. The CSD is also Hermitian, i.e.,

$$W(\boldsymbol{r}_1, \boldsymbol{r}_2) = W^*(\boldsymbol{r}_2, \boldsymbol{r}_1). \tag{2.11}$$

This, for example, means it is enough to measure only one half of the matrix of a sampled CSD data array. A useful criterion to recognize a genuine CSD is that all of them can be expressed in the form

$$W(\boldsymbol{\rho}_1, \boldsymbol{\rho}_2) = \int_{\infty}^{\infty} p(\boldsymbol{v}) H^*(\boldsymbol{\rho}_1, \boldsymbol{v}) H(\boldsymbol{\rho}_2, \boldsymbol{v}) \, \mathrm{d}^2 v, \tag{2.12}$$

where $H(\boldsymbol{\rho}, \boldsymbol{v})$ is an arbitrary kernel and $p(\boldsymbol{v})$ is a non-negative function [10, 11].

Strictly speaking, in the case of narrow-band fields such as those emitted by multimode lasers, we do not usually measure the CSD since frequency-resolved measurements are difficult. Instead, we measure its frequency-integrated form

$$J(\boldsymbol{\rho}_1, \boldsymbol{\rho}_2) = \int_{0}^{\infty} W(\boldsymbol{\rho}_1, \boldsymbol{\rho}_2, \omega) \, \mathrm{d}\omega, \tag{2.13}$$

known as the mutual intensity. In Papers **I** and **II** we indeed used mutual intensity $J(\boldsymbol{\rho}_1, \boldsymbol{\rho}_2)$ as the measure of spatial coherence. Nevertheless, in this thesis we call all measured coherence functions CSD for consistency, as all light sources we are studying are at least quasimonochromatic. Also, when calculating the propagation of different field modes, which (unless degenerate) are centered at different frequencies, we should in principle treat every individual wavelength individually to be exact. However, the error made by using only the central wavelength is negligible.

Let us now introduce an angular form of the CSD, known as the angular cross-correlation function (ACF), defined as

$$A(\boldsymbol{\kappa}_1, \boldsymbol{\kappa}_2) = \iint_{-\infty}^{\infty} W(\boldsymbol{\rho}_1, \boldsymbol{\rho}_2) \exp\left[-\mathrm{i}(\boldsymbol{\kappa}_1 \cdot \boldsymbol{\rho}_1 - \boldsymbol{\kappa}_2 \cdot \boldsymbol{\rho}_2)\right] \, \mathrm{d}^2\rho_1 \, \mathrm{d}^2\rho_2, \tag{2.14}$$

where $\boldsymbol{\kappa} = \left(k_x, k_y\right)$ is the transverse componet of the wave vector $\boldsymbol{k} = \left(k_x, k_y, k_z\right)$. We may now define the angular spectral density as

$$F(\boldsymbol{\kappa}) = A(\boldsymbol{\kappa}, \boldsymbol{\kappa}) \tag{2.15}$$

and the complex degree of angular coherence

$$\mu(\boldsymbol{\kappa}_1, \boldsymbol{\kappa}_2) = \frac{A(\boldsymbol{\kappa}_1, \boldsymbol{\kappa}_2)}{\left[F(\boldsymbol{\kappa}_1, \omega) F(\boldsymbol{\kappa}_2)\right]^{1/2}} \tag{2.16}$$

in analogy with their counterparts in the spatial domain. In the far zone the CSD is then [1]

$$W^{\infty}(r_1 \boldsymbol{s}_1, r_2 \boldsymbol{s}_2) = (2\pi k)^2 \cos\theta_1 \cos\theta_2 A(\boldsymbol{\sigma}_1, \boldsymbol{\sigma}_2) \frac{\exp[\mathrm{i}k(r_1 - r_2)]}{r_1 r_2}, \tag{2.17}$$

where $r = |\boldsymbol{r}|$, $\boldsymbol{s} = \boldsymbol{r}/r$ is the unit position vector, $\boldsymbol{\sigma} = \left(s_x, s_y\right) = (x/r, y/r)$ is its transverse component, θ is the angle between $\boldsymbol{s}$ and the z axis, and $k = 2\pi/\lambda$ is the wave number. The function

$$J(r\boldsymbol{s}) = r^2 W^{\infty}(r\boldsymbol{s}, r\boldsymbol{s}) = (2\pi k)^2 \cos^2\theta F(\boldsymbol{\sigma}), \tag{2.18}$$

known as the radiant intensity, describes the angular distribution of optical intensity in the far zone.

The theory presented above for scalar fields can be expanded to vectorial electromagnetic fields [12], which leads to the concept of a cross-spectral tensor and allows one to study the combined effects of partial coherence and partial polarization. In this thesis we consider only linearly polarized light fields, which are reasonably directional. In such circumstances the scalar approach, in which only one field component is considered, is a good model.

2.2 COHERENT-MODE DECOMPOSITION

When propagation problems with two-dimensional fields are considered, dealing with the CSD directly usually leads to numerically untractable problems; Eqs. (2.14)–(2.18) show that four-dimensional integrals need to be evaluated. Luckily, any CSD may be represented as an incoherent sum of coherent modes, which reduces the propagation formulas in sums of two-dimensional integrals. Specifically, we may write the field across the source plane in the form of a Mercer-type coherent-mode expansion [13]

$$W(\boldsymbol{\rho}_1, \boldsymbol{\rho}_2) = \sum_m c_m v_m^*(\boldsymbol{\rho}_1) v_m(\boldsymbol{\rho}_2), \tag{2.19}$$

where c_m are real and nonnegative weight factors and $v_m(\boldsymbol{\rho})$ are the modal wave functions. If the CSD is known, these weights and mode functions can be found evaluating the eiqenvalues and eiqenfunctions of the Fredholm integral equation

$$\int_{-\infty}^{\infty} W(\boldsymbol{\rho}_1, \boldsymbol{\rho}_2) v_m(\boldsymbol{\rho}_1) \mathrm{d}^2\rho_1 = c_m v_m(\boldsymbol{\rho}_2). \tag{2.20}$$

Once the eigenvalues and eigenmodes are known for the field at the source plane, the propagated CSD

$$W(\boldsymbol{r}_1, \boldsymbol{r}_2) = \sum_m c_m v_m^*(\boldsymbol{r}_1) v_m(\boldsymbol{r}_2) \tag{2.21}$$

can be evaluated using the standard two-dimensional propagation integrals for fully coherent light to relate the modal contributions $v_m(\boldsymbol{r})$ to $v_m(\boldsymbol{\rho})$.

Considering y-invariant fields, the numerical solution of the eigenvalues and modes from Eq. (2.20) involves discretizing the CSD $W(x_1, x_2)$ and solving the matrix equation

$$\mathbf{W} = \mathbf{V}\mathbf{I}\mathbf{V}^{-1}, \tag{2.22}$$

where $\mathbf{W}$ contains the CSD data, the columns of $\mathbf{V}$ are the eigenmodes, $\mathbf{I}$ is a diagonal matrix with corresponding eigenvalues, and all three are $N \times N$ square matrices if N modes are retained in

Eq. (2.20). This equation can be solved using standard numerical libraries found in many software packages such as Matlab [14]. For two-dimensional sources with four-dimensional CSDs $W(\boldsymbol{\rho}_1, \boldsymbol{\rho}_2)$ the task becomes more demanding, and might require custom numerical functions. Fortunately, in some important special cases the modes and their weights are known analytically.

2.3 SCHELL-MODEL SOURCES

Many light sources obey the Schell model, where the complex degree of spatial coherence does not depend on absolute positions $\boldsymbol{\rho}_1$ and $\boldsymbol{\rho}_2$, but only on their difference $\Delta\boldsymbol{\rho} = \boldsymbol{\rho}_2 - \boldsymbol{\rho}_1$. In this case the CSD has the form [15]

$$W(\boldsymbol{\rho}_1, \boldsymbol{\rho}_2) = [S(\boldsymbol{\rho}_1) S(\boldsymbol{\rho}_2)]^{1/2} \mu(\Delta\boldsymbol{\rho}). \tag{2.23}$$

This is convenient for coherence measurements since one would not have to measure all coherence between all combinations of the coordinates, which for a two-dimensional planar source would mean a four-dimensional matrix. Instead, it is enough to vary just the separation between the measurement points.

It is also possible to define sources that are of the Schell-model form in the space-frequency domain. In this case we write the ACF in a form analogous to Eq. (2.23), i.e.,

$$A(\boldsymbol{\kappa}_1, \boldsymbol{\kappa}_2) = [F(\boldsymbol{\kappa}_1) F(\boldsymbol{\kappa}_2)]^{1/2} \gamma(\Delta\boldsymbol{\kappa}), \tag{2.24}$$

where $\Delta\boldsymbol{\kappa} = \boldsymbol{\kappa}_2 - \boldsymbol{\kappa}_1$. Hence the complex degree of angular coherence, $\gamma(\Delta\boldsymbol{\kappa})$, now depends only on the difference between the two spatial-frequency vectors.

2.4 SHIFTED ELEMENTARY-FIELD METHOD

While the coherent-mode representation can model any arbitrary field, finding the coherent modes is usually a very demanding task, with only a few analytical solutions being known. We therefore proceed to describe another method, which deals with a specific

class of genuine CSDs but is nevertheless applicable to wide variety of cases (if not exactly, at least to a good approximation).

In late 1970s Gori and Palma introduced a method to model Gaussian Schell-model sources [16, 17] using a set of laterally or angularly shifted 'elementary' modes, which can be summed incoherently to form the correct CSD. This model was later extended to more general planar sources [18], three-dimensional sources [19], partially temporally coherent pulse trains [20], and vectorial electromagnetic sources [21]. A review of this elementary-mode method can be found in [22]. The elementary-field method has been applied, e.g., to analyzed excitation of surface plasmons under partially coherent illumination [23], beam shaping problems with various types of illumination and shaping elements [24,25], and optical imaging problems [26].

Considering the formulation of the elementary-field method in the spatial domain, we assume that the CSD at the source plane can be represented as

$$W(\boldsymbol{\rho}_1, \boldsymbol{\rho}_2) = \int_{-\infty}^{\infty} p(\boldsymbol{\rho}') f^*(\boldsymbol{\rho}_1 - \boldsymbol{\rho}') f(\boldsymbol{\rho}_2 - \boldsymbol{\rho}') \, \mathrm{d}^2\rho', \tag{2.25}$$

which implies that its spectral density is given by

$$S(\boldsymbol{\rho}) = \int_{-\infty}^{\infty} p(\boldsymbol{\rho}') |f(\boldsymbol{\rho} - \boldsymbol{\rho}')|^2 \, \mathrm{d}\boldsymbol{\rho}'. \tag{2.26}$$

Here $f(\boldsymbol{\rho})$ is a well-behaved function called the elementary field mode and $p(\boldsymbol{\rho}')$ a non-negative weight function. This means that the field is expressed as sum of identical but spatially shifted and weighted modes. Clearly, Eq. (2.25) represent a genuine CSD since it is a special case of Eq. (2.12): now $p(\boldsymbol{\rho}')$ takes the role of $p(\boldsymbol{v})$ and $f(\boldsymbol{\rho} - \boldsymbol{\rho}')$ that of $H(\boldsymbol{\rho}, \boldsymbol{v})$.

It is a simple matter to show, using Eq. (2.14), that if the source-plane field is of the form of Eq. (2.25), the angular cross-correlation function obeys the Schell model (2.24) provided that

$$f(\boldsymbol{\rho}) = \frac{1}{(2\pi)^2} \int_{-\infty}^{\infty} [F(\boldsymbol{\kappa})]^{1/2} \exp(\mathrm{i}\boldsymbol{\rho} \cdot \boldsymbol{\kappa}) \, \mathrm{d}^2\kappa \tag{2.27}$$

and

$$p(\boldsymbol{\rho}') = \frac{1}{(2\pi)^2} \int_{-\infty}^{\infty} \gamma(\Delta\boldsymbol{\kappa}) \exp(\mathrm{i}\boldsymbol{\rho}' \cdot \Delta\boldsymbol{\kappa}) \, \mathrm{d}^2\Delta\kappa. \tag{2.28}$$

In view of Eq. (2.27), the elementary field can be determined directly from the angular spectral density, which is an easily measurable quantity. The determination of the weight function generally requires spatial coherence measurements in the far zone, which may in practice be a difficult task. This task is, however, greatly simplified if the source is known to be quasihomogeneous, i.e., its spatial coherence area is small compared to the source size. In this case one may use the source-plane intensity profile directly as the weight function since $S(\boldsymbol{\rho}) \approx p(\boldsymbol{\rho})$ [18].

2.5 SUMMARY

The cross-spectral density function (CSD) is a nonnegative definite function that fully defines the spatial coherence properties of spatially partially coherent light. Even though the CSD is an important mathematical concept, its direct numerical handling in, e.g., propagation problems is often too difficult. Therefore it is useful to represent the CSD in terms of sums of coherent modes introduced in this Chapter. The Mercer-type coherent-mode decomposition is fully accurate, but its determination can in many cases be a rather heavy task. On the other hand, the elementary-field representation is numerically highly efficient whenever it is applicable.

3 Model sources and fields

In this Chapter we introduce a useful idealized model for spatially partially coherent light sources, known as the Gaussian Schell model (GSM) [15]. This model is capable of describing several real partially coherent sources and beams generated by them in an approximate way, including excimer [27] and free-electron [28, 29] lasers beams and, as we will see in Chapter 4, also widely diverging fields emanating from broad-area laser diodes (Papers I and II). Both coherent-mode and elementary-field representation are shown to be applicable to GSM sources. The propagation of fields generated by GSM sources can be governed analytically [30], but we also consider numerical modeling of their propagations. This will allow us to assess the accuracy of finite or discrete modal representations, providing useful yardsticks for numerical modeling light propagation from more complicated realistic sources including broad-area laser diodes to be considered later on in this thesis.

In the case of GSM sources, the coherent modes have a mathematical form of Hermite–Gaussian modes generated in spherical-mirror resonators [31, 32], with a specific set of modal weights [33, 34]. Other model sources that do not generally obey the Schell model can be constructed using different sets of modal weights: multi-spatial-mode lasers in either gas, solid-state, or semiconductor form can all emit such spatially partially coherent radiation. On the other hand, GSM sources have an elementary-field expansion, which involves a Gaussian elementary field with a Gaussian weight distribution. Retaining the assumption that the elementary field is still Gaussian but letting the weight profile be more arbitrary again leads to useful generalizations with spatial profiles and spatial coherence functions that are not Gaussian form. In Chapter 4 such a model will be applied to multimode broad-area edge-emitting semiconductor lasers.

3.1 GAUSSIAN SCHELL MODEL SOURCES

The most widely used model source in the theory of spatially partially coherent optics is undoubtedly the GSM source, which generates GSM fields that may exhibit widely different divergence properties depending on the chosen combination of the source parameters. In this model both the spectral density and the degree of spatial coherence at the source plane have Gaussian shapes. The most prominent features of the GSM beams are that their shape stays constant as they propagate. Their propagation behavior can be determined analytically using the same kind of propagation parameters that are employed to describe the fully coherent Gaussian beams, as shown explicitly in Ref. [30]. Indeed, GSM beams can be seen as natural generalizations of traditional Gaussian beams into the domain of spatially partially coherent optics.

In what follows, we first describe the properties of a GSM source (or the waist of a GSM beam). Since the CSD of a GSM beam is separable in transverse coordinates, we only consider its representation in the x-direction, with the understanding that a strictly similar description is valid in the y-direction as well. In the case of anisotropic GSM beams [35, 36], the parameters that define the source size and its coherence area are generally different in x and y directions.

Consider the general representation of a Shell-mode source described by Eq. (2.23). When written in a y-invariant form, this expression reads as

$$W(x_1, x_2) = [S(x_1)S(x_2)]^{1/2}\, \mu(\Delta x). \tag{3.1}$$

The GSM source is described by Gaussian distributions of the spectral density and degree of spatial coherence: we may write

$$S(x) = S_0 \exp\left(-\frac{2x^2}{w_0^2}\right) \tag{3.2}$$

and

$$\mu(\Delta x) = \exp\left(-\frac{\Delta x^2}{2\sigma_0^2}\right), \tag{3.3}$$

where w_0 and σ_0 are the characteristic widths of the intensity profile and degree of spatial coherence, respectively. Figure 3.1 illustrates the full CSD and the complex degree of coherence (in this case real-valued) of a one-dimensional GSM source when plotted as a function of the absolute coordinates x_1 and x_2.

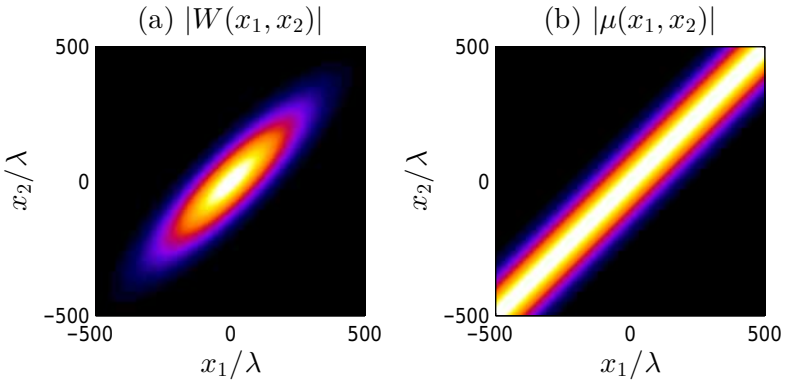

Figure 3.1: Coherence properties of a Gaussian Schell-model source. The cross-spectral density function (left) and the complex degree of spatial coherence (right) when $w_0 = 300\lambda$ and $\sigma_0 = 80\lambda$.

When a beam radiated by a GSM source propagates in free space, its intensity distribution remains Gaussian, but the transverse scale expands according to the law

$$w(z) = w_0 \left[1 + (z/z_\mathrm{R})^2\right]^{1/2}, \tag{3.4}$$

where

$$z_\mathrm{R} = \frac{\pi w_0^2}{\lambda}\beta \tag{3.5}$$

and

$$\beta = \left[1 + (w_0/\sigma_0)^2\right]^{-1/2}. \tag{3.6}$$

The absolute value of the complex degree of coherence also remains Gaussian, but the width σ_0 at the source plane is replaced with $\sigma(z)$. An important feature of GSM beams is that ratio of the beam width

and coherence width stays constant as the beam propagates, i.e.,

$$\alpha = \frac{\sigma_0}{w_0} = \frac{\sigma(z)}{w(z)} \tag{3.7}$$

is a propagation-invariant quantity. While being real-valued at the source plane, the complex degree of coherence acquires a quadratic phase as the beam propagates [30]. In Chapter 5.3 we will introduce some extensions to this basic Gaussian Schell-model beam.

3.1.1 Coherent-mode representation

Even though the free-space propagation of the GSM beam can be governed analytically, the situation is different if the beam is disturbed by any object such as a simple aperture. The propagation of such a disturbed beam must be evaluated numerically and then it is convenient to represent the source in terms of its coherent modes. The coherent-mode expansion of the GSM source is

$$W(x_1, x_2) = \sum_{m=0}^{\infty} c_m v_m^*(x_1) v_m(x_2). \tag{3.8}$$

The eigenfunctions are of Hermite–Gaussian form [33, 34]

$$v_m(x) = \left(\frac{2}{\pi w_0^2 \beta}\right)^{1/4} \frac{1}{(2^m m!)^{1/2}} H_m\left(\frac{\sqrt{2}x}{w_0\sqrt{\beta}}\right) \exp\left(-\frac{x^2}{w_0^2\beta}\right), \tag{3.9}$$

where $H_m(x)$ is a Hermite polynomial of order m, and the eigenvalues (or weights of the modes) are

$$c_m = S_0 \sqrt{2\pi} w_0 \frac{\beta}{1+\beta} \left(\frac{1-\beta}{1+\beta}\right)^m. \tag{3.10}$$

When the beam propagates in free space, the eigenmodes expand laterally and acquire a quadratic phase in precisely the same way as the modes emanating from a spherical-mirror resonator.

3.1.2 Elementary-field representation

An alternative way to model GSM sources is the shifted elementary mode method. Now the CSD function is expressed in the form analogous to Eq. (2.25), as

$$W(x_1, x_2) = \int_{-\infty}^{\infty} p(x') f^*(x_1 - x') f(x_2 - x') \, \mathrm{d}x'. \tag{3.11}$$

The elementary modes $f(x)$ and their weight function $p(x')$ both have Gaussian shapes

$$f(x) = f_0 \exp\left(-\frac{x^2}{w_\mathrm{e}^2}\right) \tag{3.12}$$

and

$$p(x') = p_0 \exp\left(-\frac{2x'^2}{w_\mathrm{p}^2}\right). \tag{3.13}$$

Their widths depend on the original beam and coherence widths of the beam according to [22, 37].

$$w_\mathrm{p} = w_0 \sqrt{1 - \beta^2} \tag{3.14}$$

and

$$w_\mathrm{e} = w_0 \beta. \tag{3.15}$$

The elementary field, of course, propagates in free space according to the usual propagation laws for fully coherent Gaussian beams.

3.2 CROSS-SPECTRAL DENSITY WITH FINITE NUMBER OF MODES

In numerical modeling one must truncate the coherent-mode representation of the GSM source by including only modes up to $m = M$ in Eq. (3.8), with M chosen large enough to represent the field with a sufficient accuracy; the effective number of modes of a partially coherent field is analyzed in Ref. [38]. The results with a finite number of modes are illustrated in Fig. 3.2, where the properties of the

GSM source are analyzed using five lowest-order coherent modes and assuming the same parameters as in Fig. 3.1. The inclusion of five modes is quite sufficient to represent the intensity distribution $S(x)$ well, as seen from Fig. 3.2(c). Also the CSD plot in Fig. 3.2(a) is nearly identical to the ideal result shown in Fig. 3.1(a). When the complex degree of coherence is considered, clear differences between the finite approximation in Fig. 3.2(b) and the exact result shown in Fig. 3.1(b) are seen. However, these are significant only in regions where the beam intensity is low.

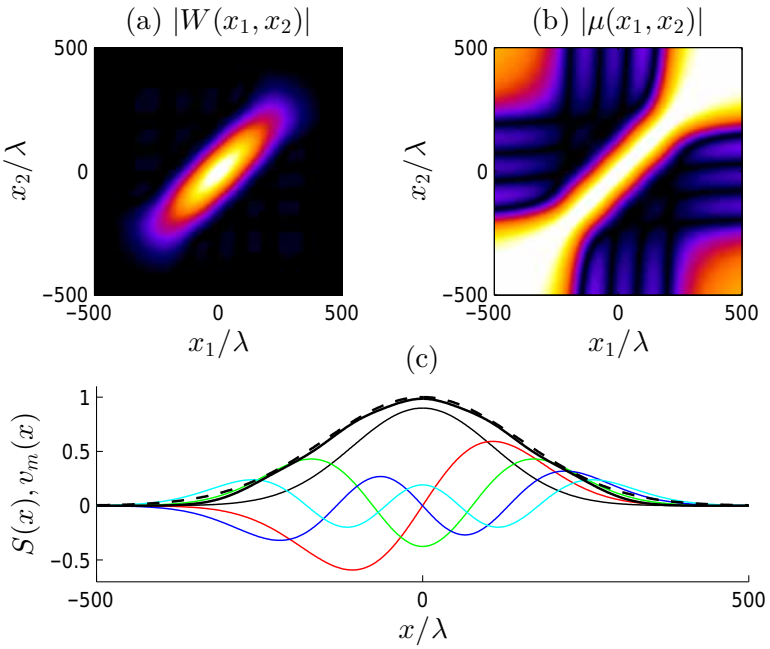

Figure 3.2: Representation of a GSM source with a finite number of coherent modes. (a) Cross-spectral density function. (b) Complex degree of spatial coherence. (c) Field profiles of some lowest-order eigenmodes (thin black, red, blue and cyan lines), the intensity profile $S(x)$ with five modes included (thick solid line), and the exact Gaussian intensity profile (dashed line).

The number of modes that need to be included in the coherent-mode representation depends on the degree of coherence of the source, characterized by the parameter β. In view of Eq. (3.10), we

have

$$\frac{c_m}{c_0} = \left(\frac{1-\beta}{1+\beta}\right)^m \tag{3.16}$$

Therefore, denoting by M the index of the highest-order coherent mode included in the numerical analysis, we have $c_M/c_0 < R$ if

$$M > \frac{\log R}{\log\left[(1-\beta)/(1+\beta)\right]}. \tag{3.17}$$

We have found that the choice $R = 0.05$ is sufficient to ensure numerical convergence. Hence the required value of M can be determined from Eq. (3.17) for a GSM source of any state of coherence.

In numerical calculations with the elementary-field representation the integral in Eq. (3.11) need to be replaced by a discrete sum, i.e., the CSD is written in the form

$$W(x_1, x_2) = \sum_{m=-M}^{M} p(m\Delta x) f^*(x_1 - m\Delta x) f(x_2 - m\Delta x). \tag{3.18}$$

Figure 3.3 illustrates the properties of the CSD with the same parameters w_0 and σ_0 as in Fig. 3.1. The separation between the adjacent elementary modes is chosen as $\Delta x = 90\lambda = 1.125\sigma_0$, and $M = 5$. Clearly, with these parameters the intensity profile $S(x)$ has not yet converged to the Gaussian shape. Hence Δx should be reduced further. Also the CSD and the complex degree of spatial coherence shown in Figs. 3.3(a) and 3.3(b), respectively, differ significantly from the ideal shapes in Figs. 3.1(a) and 3.1(b). The fluctuations in the direction of the average spatial coordinate $x = \frac{1}{2}(x_1 + x_2)$ indicate that the finite representation does not approximate the Schell model adequately well yet.

To obtain convergent results with the elementary-field method, the sampling interval Δx must be small enough and the value of M large enough to represent the field properly. Our numerical simulations show that the choices

$$\Delta x < 0.8\sigma_0 \tag{3.19}$$

and

$$M > 1.5w_0/\Delta x \tag{3.20}$$

ensure adequate convergence of the results.

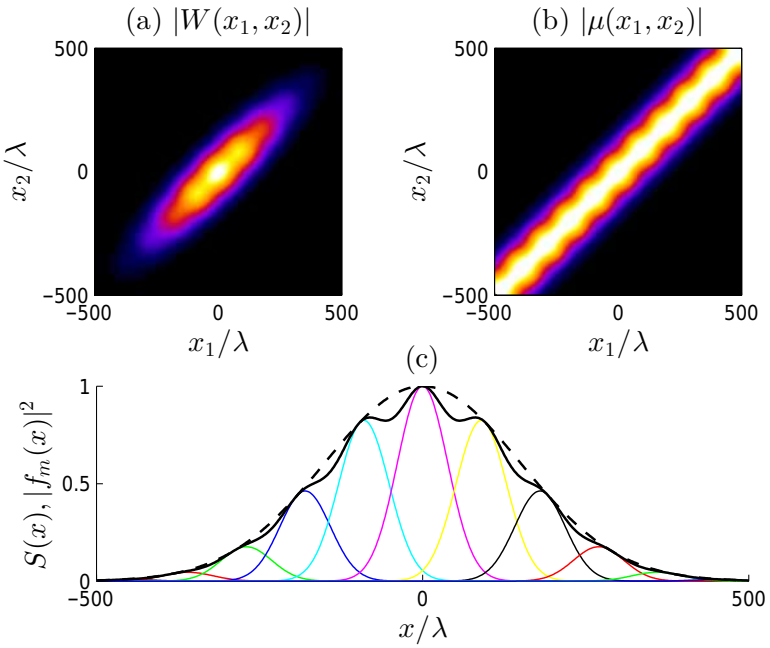

Figure 3.3: Representation of a GSM source with a finite number of shifted elementary modes. (a) Cross-spectral density function. (b) Complex degree of spatial coherence. (c) Field profiles of some elementary modes (thin lines), the intensity profile $S(x)$ with 11 elementary modes included (thick solid line), and the exact Gaussian intensity profile (dashed line).

3.3 SUMMARY

In this Chapter the Gaussian Schell model was presented as a useful tool for approximate description of many real spatially partially coherent sources. Also the coherent-mode and elementary-field representations of GSM sources were introduced. In addition, the effects of including only a finite number of modes were illustrated numerically.

4 Real sources: modeling and measurement

In the previous Chapter we discussed ideal source models, whereas in this Chapter we will introduce certain real-life partially coherent light sources. Methods for characterization of their spatial coherence properties are discussed and experimental results are given.

4.1 PARTIALLY COHERENT LIGHT SOURCES

To be exact, there are no light source that are spatially fully coherent or completely incoherent, though single-mode lasers can be considered as fully coherent sources for all practical purposes and thermal sources as well as surface-emitting light-emitting diodes (LEDs) have spatial coherence areas with dimensions in the scale of the wavelength. There are several important laser sources with partial spatial coherence properties, including excimer lasers [27], free-electron lasers [28,29,39], many vertical-cavity surface-emitting laser (VCSEL) arrays [40–43], and random lasers [44,45]; see Ref. [37] for a more thorough discussion. Also multimode edge-emitting semiconductor lasers are spatially partially coherent, and they will be considered in more detail below.

4.1.1 Broad area laser diodes

The class of partially coherent light sources we concentrate on are Broad Area Laser Diodes (BALDs), which are high-power edge-emitting semiconductor light sources [46–50]. Figure 4.1 sketches the shape of the resonator and the asymmetric spreading of the BALD beam. We denote the resonator dimensions by L_x, L_y, and L_z. The main difference between BALDs and typical laser diodes used in, e.g., telecommunication applications is the much wider

resonator cavity of BALDs. Typically $L_x \sim 100$ μm, which allows a large number of lateral modes to be excited and therefore facilitates high output power. However, as the modes are mutually uncorrelated, this also leads to a low degree of spatial coherence and reduced beam quality [51, 52]. In y direction the resonator is much narrower ($L_y \sim 1$ μm), which allows only one mode, and hence the light in y direction is essentially spatially coherent. In modeling the spatial coherence of BALDs, we can therefore restrict our study to x direction alone.

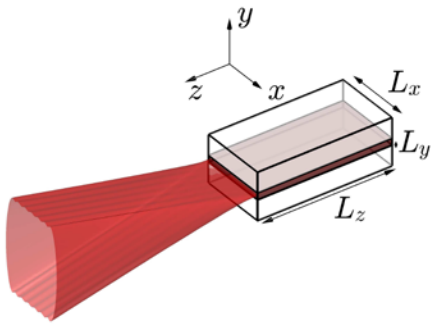

Figure 4.1: The BALD resonator and the type of beam radiated by it.

Strictly speaking, there are nanosecond-scale temporal fluctuations in the temporal intensity of BALD emission in continuous-wave operation [53–55]. Nevertheless, we can treat BALDs as stationary sources, though their temporal coherence is low because of the large number of co-existing and mutually uncorrelated longitudinal modes. We will see direct evidence of the longitudinal (as well as transverse) mode structure when studying a particular BALD experimentally in Sect. 4.2.1.

Figure 4.2 shows how the measured optical power increases linearly with driving current above the lasing threshold (at $\sim$ 600 mA). Below this threshold the BALD acts essentially as an edge-emitting LED and emits almost spatially incoherent light in x direction (while the emission remains highly coherent in y direction). When the driving current rises in the linear (lasing) region, more and more

transverse modes are excited and the coherence properties of the BALD change (Paper **II**).

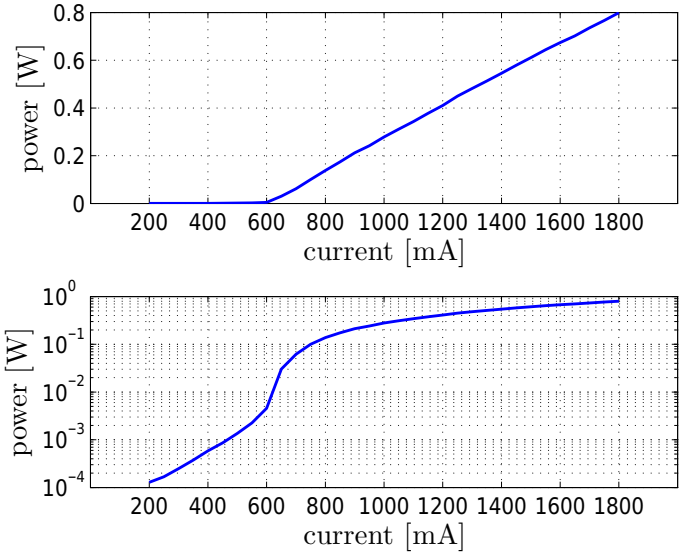

Figure 4.2: BALD power as function of the driving current in (a) linear scale and (b) in logarithmic scale.

4.1.2 Modes

In the ideal case the BALD resonator may be modeled as a planar waveguide with well-defined modes. Now, as $L_x \gg \lambda$, the tails of the modal fields outside the resonator in the x direction are insignificant, and it is enough to model the field inside the resonator as a sinusoidal wave. In other words, we treat the dielectric waveguide as a mirror waveguide with perfectly conducting mirrors at the edges $x = \pm L_x/2$. This approximation is much closer to being realistic than the use of Hermite–Gaussian modes, which may be used to approximate the exact waveguide modes in the case of narrower multimode resonators. In reality the resonator has imperfections and the shape of the modes is rather irregular, especially

with the BALD specimen we studied. Nevertheless, it is useful to model the modes at the source plane by writing

$$v_m(x) = \begin{cases} \sqrt{2/L_x}\sin(\pi m x/L_x) & \text{if } |x| \leq L_x/2 \text{ and } m \text{ is even} \\ \sqrt{2/L_x}\cos(\pi m x/L_x) & \text{if } |x| \leq L_x/2 \text{ and } m \text{ is odd} \\ 0 & \text{otherwise,} \end{cases} \tag{4.1}$$

where $m = 1, 2, 3, \ldots$ is the mode index. The modal fields in the far zone can be determined by calculating the Fourier transforms

$$a_m(k_x) = \frac{1}{2\pi}\int_{-\infty}^{\infty} v_m(x)\exp\left(-\mathrm{i}k_x x\right)\,\mathrm{d}x. \tag{4.2}$$

This gives

$$a_m(k_x) = \begin{cases} \mathrm{i}m(-1)^{m/2}\sqrt{2L_x}\dfrac{\sin(k_x L_x/2)}{\pi^2 m^2 - k_x^2 L_x^2} & \text{if } m \text{ is even} \\ m(-1)^{(m-1)/2}\sqrt{2L_x}\dfrac{\cos(k_x L_x/2)}{\pi^2 m^2 - k_x^2 L_x^2} & \text{if } m \text{ is odd} \end{cases} \tag{4.3}$$

and by plotting these we see that in the far field a single mode forms two symmetric peaks.

4.1.3 Coherence properties

The spatial coherence properties of the field can now be determined by applying the coherent-mode representation. If we assume that $M + 1$ modes are excited and have equal weights, the CSD may be written as

$$W(x_1, x_2) = \sum_{m=1}^{M} v_m^*(x_1) v_m(x_2) \tag{4.4}$$

Figure 4.3(a) illustrates the absolute value of the CSD at the source plane calculated with eight ideal modes with identical weights, whereas 4.3(b) shows the absolute value of the complex degree of spatial coherence. Obviously the BALD can be described as a Schell model source only approximately since there are some fluctuations in the diagonal direction of the $|\mu(x_1, x_2)|$ plot. The phase of the CSD is illustrated in Figs. 4.3(c) and (d). In the experiments to be

presented later (Figs. 4.8 and 4.13) the exit face of the BALD is imaged on the detector using a lens (focal length f, magnification M). Such an imaging geometry would introduce a spherical phase term of the form

$$\phi(x_1, x_2) = -\frac{k_0}{2Mf}(x_1^2 - x_2^2) = B(x_1^2 - x_2^2) \tag{4.5}$$

in the image-plane CSD. In Fig. 4.3(c) the effect of such a phase term (with $B = 3.56 \times 10^{-}5\ \mathrm{rad}/\mu\mathrm{m}^2$) is simulated, whereas in 4.3(d) this additional phase is removed and the true phase of the source-plane CSD is seen. Fig. 4.3(e) shows the intensity profile.

4.2 MEASUREMENT SYSTEMS

Measurement of spatial coherence functions of partially coherent light sources is far more complicated than intensity measurements. In some cases if we can assume to know the shape of the source modes, we can detect the mode weights from the measured intensity profile [56–60]. In more general cases the CSD has to be measured. Interferometric arrangements are usually employed, some of which will be described below. We begin, however, with a spectroscopic method that reveals some information on the mode structure of BALDs.

4.2.1 Imaging spectrometer

All longitudinal and transverse BALD modes have slightly different wavelengths. One way to measure them is an imaging spectrometer considered in Ref. [46], in the author's M.Sc. thesis [61], and in Fig. 4.4. A microscope objective f1 focuses the BALD exit face in magnified form into the aperture plane, and a second lens f2 images this on the camera. The grating spectrometer images the facet of the BALD on the detector, with different wavelengths shifted laterally, thus allowing one to view directly the spatial distribution of spectral density $S(x, \lambda)$. Double pass on the grating is used to increase the resolution of the system.

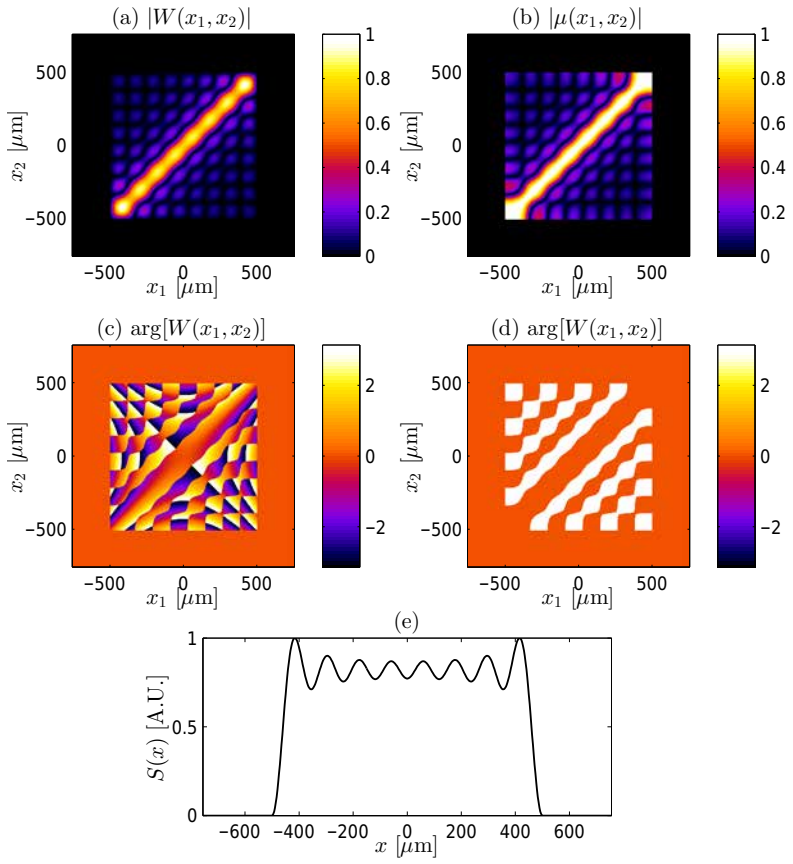

Figure 4.3: BALD coherence properties with ideal modes. Absolute values of (a) the cross spectral density function and (b) the complex degree of coherence. Phase of the CSD with (c) and without (d) a spherical component. (e) The intensity profile.

The spatial spectrum of our BALD specimen is shown in Fig. 4.5. We observe a quasi-periodic pattern with a complicated structure that roughly repeats itself at a distance $\Delta\lambda_{\mathrm{L}} \approx 0.04$ nm. This distance corresponds well to the longitudinal mode spacing of a Fabry–Perot resonator of length $L_z = 1500$ μm. The spaces between the longitudinal modes are filled (in fact overfilled) with many transverse modes, spaced in wavelength scale by $\Delta\lambda_{\mathrm{T}} \approx 0.003$ nm [61]. The structure of each transverse mode in x direction is, of

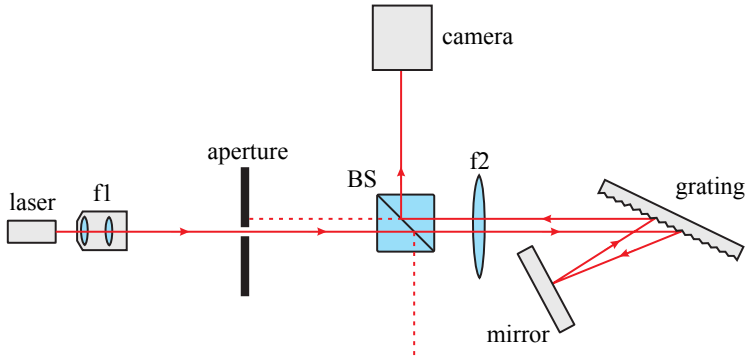

Figure 4.4: Double pass imaging spectrometer.

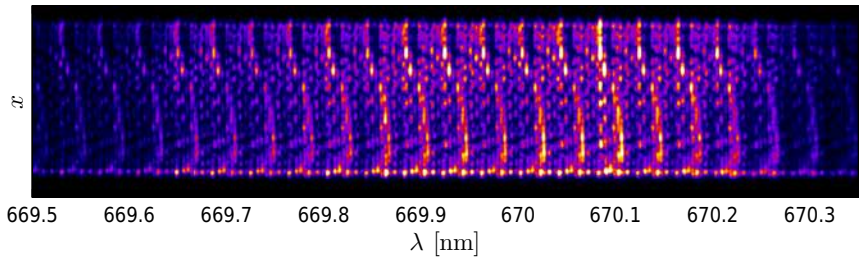

Figure 4.5: Measured spatial spectrum of the BALD.

course, different but rather difficult to judge precisely from Fig. 4.5. When comparing our measured data to corresponding results in Ref. [46], we see that the resonator and the modes of our BALD are much less ideal, and most importantly very asymmetric. Therefore simulation with the symmetric ideal modes does not work well in our case.

The advantage of the system in Fig. 4.4 is its 'immediate' operation, as the shape of every mode can be captured with a single snapshot. The disadvantages include limited resolution of the system: every mode is represented in an image of the laser facet but the transverse and longitudinal modes overlap, which makes separating the spatial modes difficult. Nevertheless this method has been used to modulate the phase profiles of BALD modes [47].

The method just described gives rough information on the mode structure but does not allow a reliable modeling of the coherence properties of BALDs. From now on we concentrate on direct measurement of spatial coherence, ignoring the finite spectral bandwidth of BALD radiation.

4.2.2 Young's double pinhole system

The classical Young's double pinhole experiment [6, 7, 62] had a major role in the acceptance of the wave nature of light in the nineteenth century. Later this setup was important in the development of coherence theory of light: the degree of spatial coherence is traditionally defined as the visibility of fringes in Young's interferometer [9]. If we position the pinholes into coordinates x_1 and x_2, we easily get the absolute value of complex degree of coherence $\mu(x_1, x_2)$, and its phase can be found from lateral shifts of the fringes. The entire CSD can be measured by scanning the pinholes over the all combinations of x_1 and x_2 and, in addition, measuring the intensity profile $S(x)$.

In paraxial approximation the intensity pattern behind the pinholes (at a sufficiently large distance, where the radiation fields from the pinholes overlap spatially) is [63]

$$\begin{aligned} S(x') = {} & S_1(x') + S_2(x') + 2[S_1(x')S_2(x')]^{1/2} \\ & \times |\mu(x_1, x_2)| \cos\left[\phi(x_1, x_2) + \frac{2\pi a}{d\lambda_0} x'\right], \end{aligned} \tag{4.6}$$

where a is the distance between the pinholes and d is the distance from the pinhole plane to the detector (see Fig. 4.6). Furthermore, S_j are the intensities detected when only pinhole j is open; S_j depend on the shape and size of the pinholes, and on the incident intensity $S(x_j)$. The origin of the coordinate axis x' is normalized to the center of the pinholes and $\phi(x_1, x_2)$ is the phase of $\mu(x_1, x_2)$. If we measure $S(x')$, $S_1(x')$, and $S_2(x')$, we may normalize the fringes

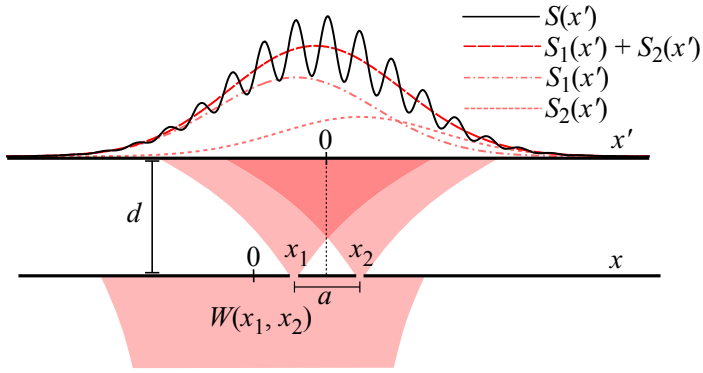

Figure 4.6: Young's double pinhole interferometer with partially coherent light.

as

$$C(x') = \frac{S(x') - S_1(x') - S_2(x')}{2[S_1(x')S_2(x')]^{1/2}} = |\mu(x_1, x_2)| \cos\left[\phi(x_1, x_2) + \frac{4\pi a}{d\lambda_0} x'\right]. \quad (4.7)$$

By fitting the sinusoidal curve on the bottom line to the measured top line, we find $|\mu(x_1, x_2)|$ and $\phi(x_1, x_2)$.

The practical problem with Young's interferometer is how to move the pinholes fast enough to scan the whole CSD within a reasonable period of time. For example, placing and aligning a new pinhole mask for each different spacing is obviously cumbersome and impractical. Several designs for more practical measurement systems has been suggested and demonstrated. For example, overlapping masks with crossed-slit apertures moved with mechanical translation stages were used in [64]. Light could also be coupled into two moving optical fibers [65–67]. A reversed-wavefront Young interferometer, where two replicas of the measured beam are created on a pinhole mask with a beam-splitter is described in [68]. The degree of coherence at several coordinate pairs can be measured at once by analyzing the complicated fringe pattern after a mask with multiple apertures [69]. Many of these methods are still mechanically too slow to measure the two dimensional $W(x_1, x_2)$

with sufficiently dense sampling. While we assume that the measured light is quasimonochromatic and can therefore ignore the chromatic effects after the pinholes, measurement of spatial coherence of polychromatic light is also possible with special arrangements [70].

4.2.3 Interferometer realized with digital micromirror device

Digital micromirror devices (DMDs) are micromechanical spatial light modulators originally developed for digital video projectors. They can tilt each pixel between on and off positions hundreds of times per second to create shades of light, while different colors are produced by illuminating the mirrors with one of the three main colors at the time at a faster rate than the human eye can notice. However, DMDs have also been used for many other applications to measure and modify light [71–76].

We purchased and modified a Texas Instruments DLP LightCrafter projector module, and removed light source LEDs and the projector lens that were not needed in our experiments. The whole measurement system is depicted in Fig. 4.7(a). The mirrors are arranged in an array with diamond orientation as illustrated in Fig. 4.7(b), where also the focused image of BALD exit facet is shown. The pinholes (in fact slits) are rows of mirrors in coordinates x_1 and x_2, tilted towards the camera. It should be noted that the DMD works as an grating and the light is reflected into several diffraction orders, not to a single beams as shown in Fig. 4.7(a) for simplicity. A similar device could also be build using reflective or transmissive liquid crystal spatial light modulators, but the problem is their poorer contrast between dark and light pixels and possibly their slower operation compared to DMDs [77].

Figure 4.8 illustrates the measured complex-valued coherence function of the BALD operating at 1000 mA driving current, i.e., well above the lasing threshold. Figure 4.8(a) shows the absolute value $|W(x_1, x_2)|$ and 4.8(b) illustrates $|\mu(x_1, x_2)|$, and the directly measured phase is depicted in 4.8(c). Because of the imaging lens

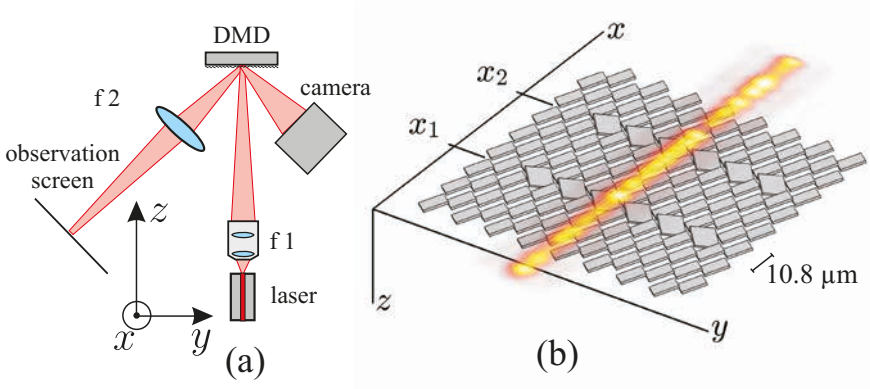

Figure 4.7: (a) The DMD-based Young's interferometer setup and (b) the arrangement of the digital micromirrors.

in the system and propagation of the beam, the phase also includes a spherical phase front. This extra phase is removed numerically in 4.8(d). Finally, the intensity profile is depicted in 4.8(e). We see that the resolution of our system is sufficient to detect even the small details of CSD. The measurement of one data point takes about one second, and scanning of the whole CSD about two hours.

In Paper **II** we describe the system in more detail and use it to characterize the BALD also with other driving currents. In Paper **III** we used the system to measure generated specular beams and in Ref. [78] to measure a beam modulated by a deterministic rotating spiral diffuser.

4.3 GAUSSIAN SCHELL MODEL BEAMS GENERATED BY ROTATING DIFFUSERS

A simple method to produce light fields with Gaussian-shaped degrees of coherence is to use a random rotating diffuser, which can be just a ground piece of glass or plastic [79]. The spread angle of scattered light depends on the roughness of the diffuser and the coherence area can be controlled by changing the laser spot size on the diffuser by the focusing lens.

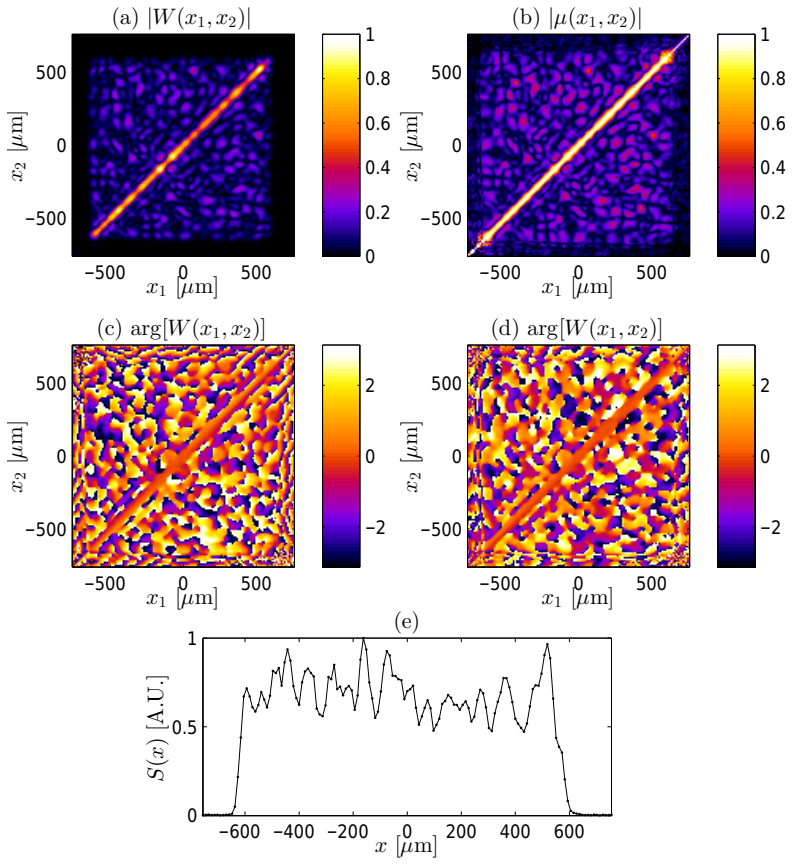

Figure 4.8: Measured BALD coherence properties. (a) Absolute value of the CSD. (b) Absolute value of the comlex degree of coherence. (c) Directly measured phase of the CSD. (d) Phase after the spherical phase is removed. (e) Measured intensity profile.

Let us assume that the Gaussian beam incident on the diffuser has an intensity profile

$$S(\boldsymbol{\rho}') = S_0 \exp\left(-\frac{2\boldsymbol{\rho}'^2}{w_{\mathrm{L}}^2}\right). \tag{4.8}$$

If the roughness scale of the diffuser is small compared to w_{L}, the time-averaged field after the diffuser can be approximately considered as a stationary, spatially incoherent secondary source. It then

follows from the vanCittert–Zernike theorem [1] that a spatially homogeneous field (with a uniform intensity distribution) is generated in the paraxial region, with a Gaussian degree of complex degree of coherence

$$\mu(\Delta\boldsymbol{\rho}) = \exp\left(-\frac{\Delta\boldsymbol{\rho}^2}{2\sigma_0^2}\right), \tag{4.9}$$

where

$$\sigma = \frac{\lambda z}{\pi w_{\mathrm{L}}}, \tag{4.10}$$

z being the propagation distance. If the scattered field is collimated by a lens of focal length $f = z$ and a Gaussian transmission filter with complex-amplitude transmittance

$$t(\boldsymbol{\rho}) = \exp\left(-\frac{\boldsymbol{\rho}^2}{w_0^2}\right) \tag{4.11}$$

is placed behind the lens, a secondary Gaussian Schell-model source characterized by parameters w_0 and σ_0 is formed [80].

It should be noted that light is detected as partially coherent only when the integration time of the detector is sufficiently large. The instantaneous intensity distribution of the scattered field is a speckle pattern, which is smoothed out when the diffuser rotates and the incident field sees different realizations of the diffuser surface.

4.4 WAVEFRONT FOLDING INTERFEROMETER

The Wavefront Folding Interferometer (WFI) is a modification of the traditional Michelson interferometer, where one or both of the mirrors is replaced with retroreflecting right-angle Porro prisms. If two prisms are used, they are placed perpendicular to each other as illustrated in Fig. 4.9. The prisms then fold the incident beam in x and y directions so that the (x, y) and $(-x, -y)$ coordinates of the original beam overlap in the output plane D. If the prisms are tilted slightly, interference fringes are seen at the D plane, and the

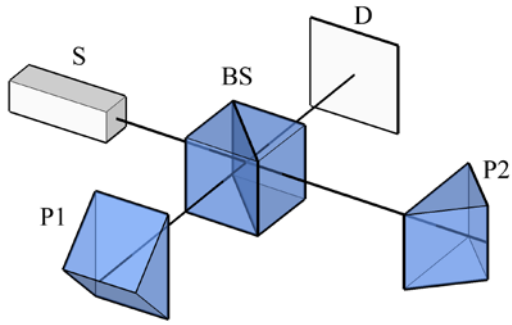

Figure 4.9: Wavefront folding interferometer. The source S generates a collimated incident beam, which is split into the parts by the beam splitter BS, folded by Porro prisms P1 and P2, an recombined before arriving at the detector D in the output plane.

visibility of these fringes can be used to measure the spatial coherence of the incident field [80–82]. The coherence of vertical-cavity surface-emitting lasers (VCSELs) was measured in with this kind of setup in Ref. [83] and slightly different configuration was used in Ref. [84]. Because of wavefront-folding nature of the interferometer, a complete coherence characterization of the CSD is possible only if the incident field is of the Schell-model form.

Figure 4.10 shows an example of interference fringes captured with a WFI with only one Porro prism. The incident field is obtained by illuminating a rotating diffuser with a ring-like intensity profile produced by an axicon [85] and a focusing lens, and thus a Bessel-correlated field [86] with a uniform-intensity distribution is incident on the WFI. More general use of axicons with partially coherent light has been discussed in Refs. [87, 88]. The horizontal line in the center of the figure is caused by the corner of the prism. More details of the experiment will be found in the forthcoming Master's thesis by Najnin Sharmin.

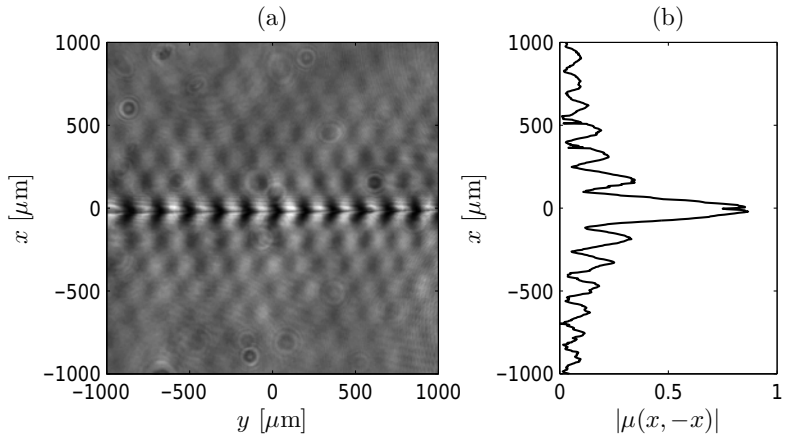

Figure 4.10: Bessel correlated light field measured with WFI. (a) Interference fringes. (b) Absolute value of the complex degree of spatial coherence.

4.5 SPECULAR BEAMS BY WAVEFRONT FOLDING INTERFEROMETER

The output light from a perfectly aligned WFI also has many interesting properties, which we studied in Paper **III**. If the prisms are not tilted, the flipped fields overlap without producing interference fringes. The output of the WFI illuminated by a coherent field v_0 is

$$v(x,y) = \frac{1}{\sqrt{2}}\left[v_0(x,-y) + v_0(-x,y)\exp\left(\mathrm{i}\phi\right)\right], \tag{4.12}$$

where ϕ is the phase difference between the fields arriving from the two interferometer arms. Therefore the output CSD has the form

$$\begin{aligned} W(x_1,y_1,x_2,y_2) = {} & \frac{1}{2}\left[W_0(x_1,-y_1,x_2,-y_2) + W_0(-x_1,y_1,-x_2,y_2)\right] \\ & + \frac{1}{2}\left[W_0(x_1,-y_1,-x_2,y_2)\exp\left(\mathrm{i}\phi\right)\right. \\ & \left. + W_0(-x_1,y_1,x_2,-y_2)\exp\left(-\mathrm{i}\phi\right)\right]. \end{aligned} \tag{4.13}$$

With choices $\phi = 2\pi n$ and $\phi = \pi/2 + 2\pi n$ the output CSD is specular or antispecular, respectively [89]. In the specular case the condition $W(-x_1,-y_1,x_2,y_2) = W(x_1,y_1,x_2,y_2)$ holds, and in the an-

tispecular case $W(-x_1, -y_1, x_2, y_2) = W^*(x_1, y_1, x_2, y_2)$, as we can readily see from Eq. (4.13).

In Paper **III** we consider in detail the case in which a Gaussian-correlated field with coherence width σ_0 is incident on the WFI. In this case a central intensity peak with characteristic width σ_0 on a uniform background is predicted in the specular case, while a central dip with the same width is predicted in the antispecular case. The CSD, when considered as a function of x_1 and x_2 (or y_1 and y_2) exhibits a distinctive cross shape with diagonal and antidiagonal arms. These features are illustrated in Fig. 4.11, which shows the theoretical values of the CSD functions of specular and antispecular beams. The top row represents the spectral density and the middle row shows the (real-valued) CSD with color scale from -2 to 2. The bottom row illustrated the (also real-valued) complex degree of coherence with color scale from -1 to 1. We see how the intensity peak and specular coherence arm disappear and transform into an intensity dip and an antispecular arm, respectively, when the value of ϕ changes. The case with $\phi = 0.5\pi$ is just the normal GSM beam. The scale of the x_1 and x_2 axes of the lower figures is the same as the x axis of the top row. The used parameters are $w_0 = 600$, $\sigma_0 = 120$, and $S_0 = 1$, in arbitrary units.

It is also shown in Paper **III** that if the WFI is illuminated by a GSM beam, the central intensity peak or dip is observed on a Gaussian background. These features survive as the output beam propagates; in fact the output beam is shape-invariant in the sense that only its scale expands upon propagation.

Figure 4.12 depicts our experimental setup. First a rotating diffuser modulates the coherent input HeNe laser beam into a partially coherent field with Gaussian coherence properties as described in Sect. 4.3. A lens f2 collimates the field into the WFI. We mounted the second prism in our setup on a piezo translation table to fine tune ϕ. Finally the DMD Young's interferometer setup introduced earlier was used to measure $W(x_1, x_2)$.

Figure 4.13 depicts measured coherence properties of a field created with the WFI. In Fig. 4.13(a) we show the absolute value of the

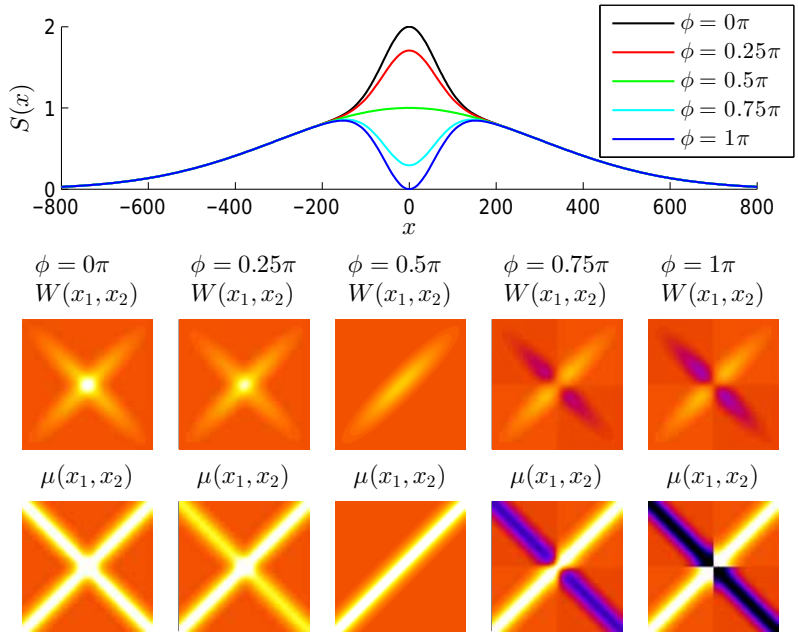

Figure 4.11: Theoretical CSD for specular and antispecular beam with five values of phase difference ϕ. Top row: spectral density, middle row CSD, bottom row: degree of coherence.

CSD, while 4.13(b) shows the absolute value of the degree of coherence. Both plots reveal the distinctive cross-shaped nature of the CSD, predicted theoretically above. Figure 4.13(c) illustrates the phase of the CSD before the spherical phase introduced by the spreading of the beam and imaging lenses is removed, and 4.13(d) shows the true phase of the CSD once this is done. Finally, Fig. 4.13(e) depicts the intensity profile of the beam measured with the interferometer system.

It should be noted that the measurement data shown in Fig. 4.13 is from early experiments, and the results demonstrate some problems we initially encountered with our experimental setup (corresponding results from later experiments are presented in Paper **III**). We measured the CSD for all (x_1, x_2) combinations without making use of the Hermiticity of the CSD, which implies the symmetry $W(x_1, x_2) = W^*(x_2, x_1)$. When we compare the top left and bottom

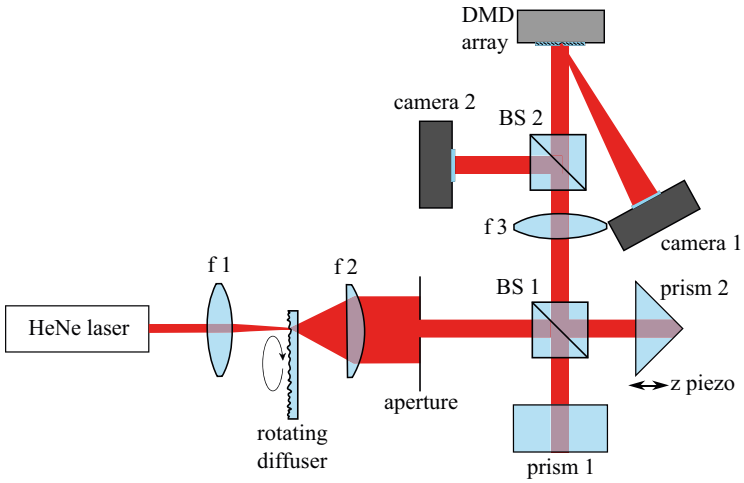

Figure 4.12: Beam modification with a wavefront folding interferometer and measurement with Young's DMD interferometer.

right corners, we see that this symmetry is slightly broken because the setup has drifted over the long measurement time. Also the wide flat right angle corner of the prism is also visible. In Paper **III** we fixed these issues by actively compensating the piezo position and using prisms with a sharper right-angle corner.

4.6 SUMMARY

Spatial coherence properties of partially coherent light sources, specifically broad-area laser diodes, were modeled and characterized experimentally using both a high-resolution imaging spectrograph and Young's interferometer realized by means of a DMD spatial light modulator. Coherence measurements and coherence modulation with a wavefront-folding interferometer were then considered. It was shown that interesting types of partially coherent fields with specular and antispecular cross-spectral density functions can be generated in this interferometric setup.

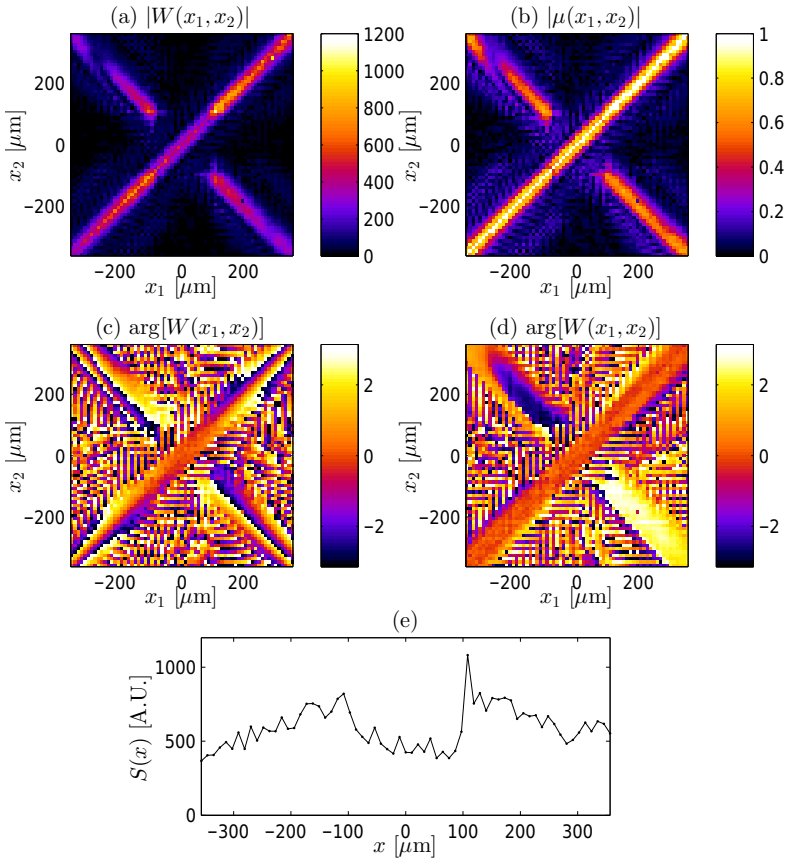

Figure 4.13: Measured properties of a WFI output field. (a) Absolute value of the CSD. (b) Absolute value of the complex degree of coherence. (c) Directly measured phase of the CSD. (d) Phase after removal of the spherical term. (e) Intensity profile.

5 Propagation and coupling of light

In the previous chapters we have discussed the modeling and measurement of partially coherent light at the primary or secondary source plane. Now we will discuss the propagation of light radiated by such sources, first in free space and then in waveguides. In particular, free-space propagation of BALD radiation and coupling of spatially partially coherent light into planar wavequides will be discussed in detail.

5.1 ANALYTICAL FORMULATION

Propagation of coherent light in free space may be governed using the angular spectrum method. Considering a y-invariant geometry, we assume that the field $v(x)$ at the source plane $z = 0$ is known. Then the field at an arbitrary distance z is given by [1]

$$v(x,z) = \int_{-\infty}^{\infty} a\left(k_x\right) \exp\left(\mathrm{i}k_x x\right) \exp\left(\mathrm{i}k_z z\right)\, \mathrm{d}k_x, \tag{5.1}$$

where $a(k_x)$ is the angular spectrum of plane waves associated with the field at $z = 0$, defined as

$$a(k_x) = \frac{1}{2\pi} \int_{-\infty}^{\infty} v\left(x\right) \exp\left(-\mathrm{i}k_x x\right)\, \mathrm{d}x. \tag{5.2}$$

Furthermore

$$k_z = \begin{cases} \sqrt{k_0^2 - k_x^2} & \text{if } |k_x| \leq k \\ \mathrm{i}\sqrt{k_x^2 - k_0^2} & \text{if } |k_x| > k \end{cases} \tag{5.3}$$

and $k_0 = 2\pi/\lambda_0$ is the vacuum wave number. Plane-wave components with real-valued k_z are homogeneous (propagating) waves, while those with imaginary-valued k_z are evanescent waves.

The angular spectrum approach can be readily expanded to propagate partially coherent light by using the definition of the CSD. We then have

$$W(x_1, x_2, z) = \iint_{-\infty}^{\infty} A\left(k_{x1}, k_{x2}\right) \exp\left[\mathrm{i}\left(k_{x2}x_2 - k_{x1}x_1\right)\right] \times \exp\left[\mathrm{i}\left(k_{z2} - k_{z1}^*\right) z\right] \,\mathrm{d}k_{x1}\,\mathrm{d}k_{x2}, \tag{5.4}$$

where

$$A(k_{x1}, k_{x2}) = \frac{1}{(2\pi)^2} \iint_{-\infty}^{\infty} W(x_1, x_2) \exp\left[\mathrm{i}\left(k_{x1}x_1 - k_{x2}x_2\right)\right] \,\mathrm{d}x_1\,\mathrm{d}x_2 \tag{5.5}$$

is the angular cross-correlation function. which was already introduced in Sect. 2.1.

Analytical solutions of this propagation integral are rare, but in fact not many are known even in the paraxial domain, where the evanescent plane-wave components can be neglected and k_z may be expressed as

$$k_z \approx k_0 - \frac{k_x^2}{2k_0}. \tag{5.6}$$

The most useful case in which an analytical paraxial solution is possible is that of a Gaussian Schell-model beam [1].

5.2 NUMERICAL IMPLEMENTATION

It is worth stressing that propagating the CSD directly is possible in the y-invariant case since only two-dimensional integrals appear in the angular spectrum representation. We may formally write (5.4) and (5.5) as

$$W(x_1, x_2, z) = \mathcal{F}_{kx2}\{\mathcal{F}_{kx1}^{-1}[A(k_{x1}, k_{x2}) \exp(\mathrm{i}k_{z1}z)] \exp(-ik_{z2}z)\} \tag{5.7}$$

and

$$A(k_{x1}, k_{x2}) = \mathcal{F}_{x2}^{-1}\{\mathcal{F}_{x1}[W(x_1, x_2)]\}, \tag{5.8}$$

where $\mathcal{F}_j$ is Fourier transform with respect to index $j = 1, 2$. The Fourier transforms involved in these expressions may be evaluated numerically using the Fast Fourier Transform algorithm.

Although direct propagation of the CSD is numerically feasible in the y-invariant case, the computations are faster if we decompose the CSD into coherent modes as described in Sections 2.2 and 2.4. Numerical issues concerning beam propagation, such as aliasing, and methods to overcome them have been discussed in [90–92].

5.2.1 Propagation of broad area laser diode beam

Let us now give a real-life example of propagation of partially coherent light with fine structural details; more details are given in Paper **II**. Propagation of a beam from our broad area laser diode with driving current 700 mA is presented in Fig. 5.1. Because light from the BALD diverges fast, we imaged the BALD output facet using a microscope objective with $10\times$ magnification. We measured the intensity profiles around the image plane ($z = 0$ in Fig. 5.1) at 1 mm intervals with a CMOS camera placed on a rail, over a region 64 mm before and 60 mm after the image plane. We normalized the intensity profiles to cancel the spreading of the beam in the y direction. The measurements reveal a highly structured field intensity distribution around the image plane.

Figure 5.1 also illustrated simulated results obtained with three different models with different levels of accuracy. Fig. 5.1(b) depicts simulated beam propagation calculated with angular spectrum method from a CSD function data measured at the image plane ($z = 0$). We first solved the coherent modes from the measurement data using Eq. (2.22), propagated them individually forwards and backwards from $z = 0$, and summed the resulting intensities incoherently. Since the CSD at the source plane is simply a $10\times$ demagnified version of this CSD, we were also able to propagate the beam upwards from the source plane ($z = -184.6$ mm) to the plane lens ($z = -167.9$ mm) and these results are also shown in the simulation. The match between the measured and simulated results is

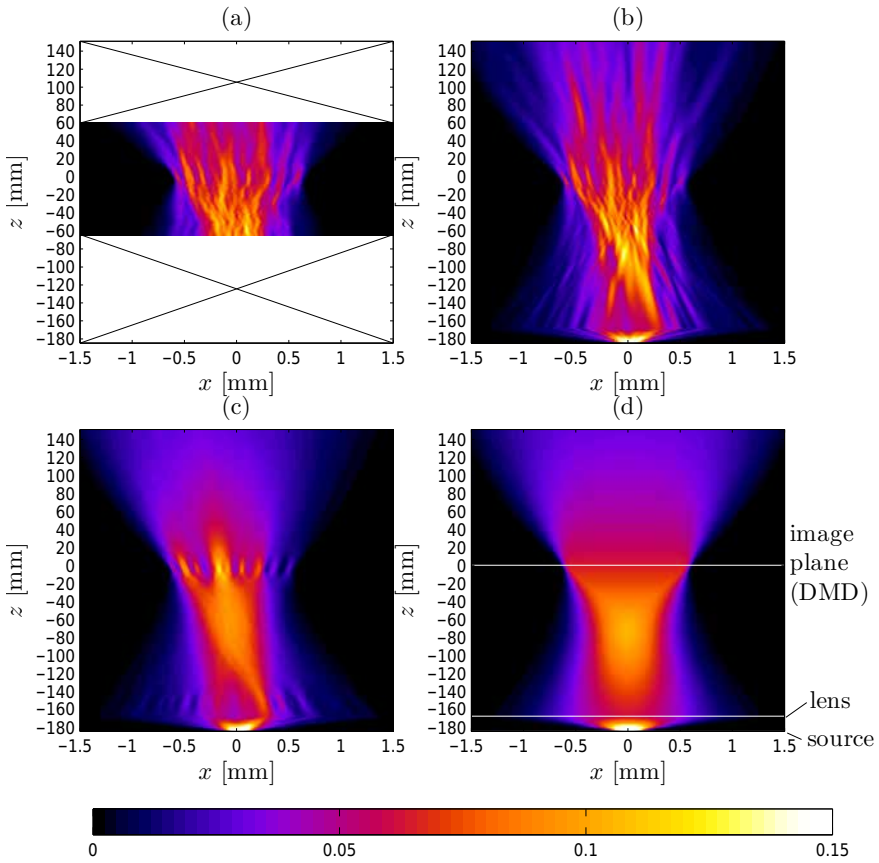

Figure 5.1: Measured and simulated BALD beam propagation with 700 mA driving current. (a) Measured intensity distribution (the crossed areas were not measured). (b) Simulated of beam propagation using the Mercer coherent-mode approach in Sect. 2.2. (c) Simulation with the shifted elementary-field representation of Sect. 2.4 using the modes and the weigh function calculated from angular and source plane intensity distributions, respectively. (d) Simulation with elementary modes with a Gaussian mode shape and a top-hat weight function.

excellent: even the small chaotic-looking details of the beam can be predicted.

We could also have propagated the field by using the measured CSD data directly since this method and the coherent-mode method are fundamentally equivalent. However, we noticed that the mea-

sured CSD is not exactly nonnegative definite because of small measurement inaccuracies. This method resulted in small (unphysical) negative intensities in some areas, but such error were quite insignificant.

The direct coherence measurement method is rather time consuming as one measurement took about two hours. In the case of two-dimensionally partially coherent fields such measurements are not possible at all unless the CSD is separable in x and y coordinates. Fortunately, if the elementary-field approach is used and the source is quasihomogeneous, one only needs to measure the source-plane (or alternatively image-plane) and far-field intensity distributions to determine the weight function and the elementary field, respectively. Figure 5.1(c) depicts simulation results using shifted elementary mode method. When modeling this kind of imaging systems the phase front of the lens has to be considered separately for elementary-field to correctly model the behavior of the beam before and after the image plane. We see that the asymmetric shape of the beam is well predicted but the small details are lost because the approach is an approximation (the BALD source does not obey exactly the assumptions of the elementary-field model). Nevertheless, the results are sufficiently accurate for most practical purposes.

In Fig. 5.1(d) we used an even simpler version of the elementary field method, assuming that the elementary field is a Gaussian beam with a spread angle that best matches the measured angular intensity distribution, and the weight is a simple top-hat function with a width of the BALD resonator. Naturally this method does not predict the asymmetry of the beam, but the over all spreading matches well. The most suitable method should be selected by considering the accuracy requirements of the application in hand.

Figure 5.2 illustrates similar simulations with 500 mA driving current of the BALD, which is below the lasing threshold and therefore the BALD operates essentially as a edge-emitting LED. Unfortunately, directly measured propagated intensity data was not available in this case. All three methods now give very similar results, indicating that for truly quasihomogeneous low-coherence

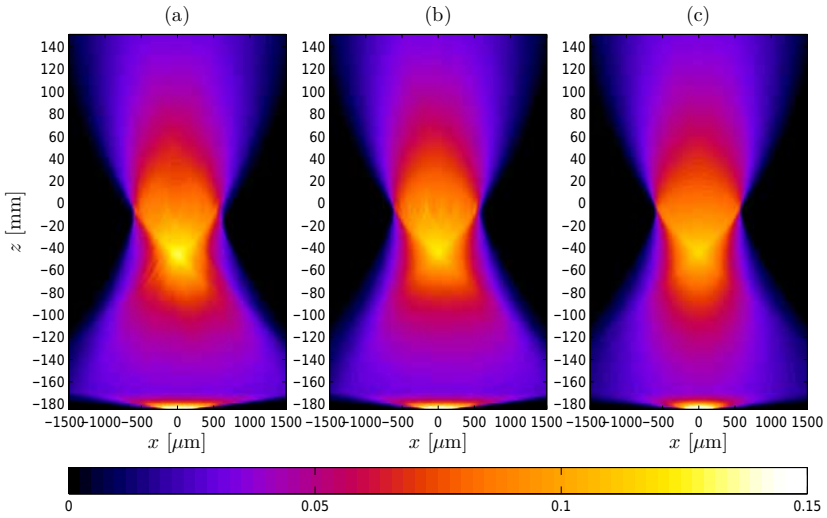

Figure 5.2: Simulated BALD beam propagation with 500 mA driving current. (a) Coherent-mode method. (b) Shifted elementary field method. (c) Elementary-field method with a Gaussian mode shape and a top-hat weight function.

sources (such as LEDs), the elementary field method gives very accurate simulation results. In this case very little knowledge about the source is required.

5.3 COUPLING INTO PLANAR WAVEGUIDES

So far we have considered light propagation in free space, but now proceed to discuss the use of the coherent-mode representation of partially coherent fields to simulate end-butt coupling of light into a planar waveguide and the propagation inside it. Partial coherence in waveguides and fibers has been studied for several decades [93–96]. More detailed results on the topic considered in this Section are given in Paper **IV**.

For simplicity we assume that entire geometry (including the incident field) is y invariant. Then each propagating mode inside the guide has a propagation-invariant form

$$u_m(x,z) = X_m(x)\exp\left(\mathrm{i}\beta_m z\right), \tag{5.9}$$

where real-valued and orthogonal function $X_m(x)$ describe the spatial shapes of the modes and β_m are their propagation constants. Let us assume that the front end of the waveguide is located at the plane $z = 0$ and assume that the CSD at this plane is given by Eq. (3.8), i.e.,

$$W(x_1, x_2) = \sum_{n=0}^{\infty} c_n v_n^*(x_1) v_n(x_2), \tag{5.10}$$

with known modal shapes $v_n(x)$ and weights c_n. If we ignore the reflection from the waveguide interface, then a part of the light is coupled into propagating modes and the rest into radiating modes. Each coherent-mode contribution to the incident CSD can now be expanded in terms of the waveguide modes as

$$\sqrt{c_n} v_n(x) = \sum_{m=0}^{M-1} p_{nm} X_m(x) + \text{radiation modes} \tag{5.11}$$

where M is the number of the guided modes supported by the waveguide. Every incoming coherent mode may generally couple to several guide modes; therefore a group of suitably weighted guide modes corresponds to a single input mode. The guided modes are mutually coherent and therefore interfere with each other, but incoherent compared to groups corresponding to other input modes.

The way input and guided field modes couple depends on how well their spatial shapes match. We get the weights p_{nm} by evaluating the overlap integral [63]

$$p_{nm} = \sqrt{c_n} \int_{-\infty}^{\infty} v_n(x) X_m(x) \mathrm{d}x. \tag{5.12}$$

If the waveguide is weakly modulated this method gives accurate results [97]. Now the CSD inside the guide at any distance $z > 0$ inside the waveguide is

$$W_{\mathrm{g}}(x_1, x_2, z) = \sum_{n=0}^{\infty} \sum_{m=0}^{M-1} \sum_{q=0}^{M-1} p_{nm}^* p_{nq} \times X_m(x_1) X_q(x_2) \exp\left[-\mathrm{i}\left(\beta_m - \beta_q\right) z\right]. \tag{5.13}$$

If we have a symmetric waveguide with guide-layer thickness d and the following refractive index distribution

$$n(x) = \begin{cases} n_\mathrm{g} & \text{if } |x| < d/2 \\ n_\mathrm{c} & \text{if } |x| > d/2, \end{cases} \tag{5.14}$$

the TE-polarized modes have the form [63]

$$X_m(x) = \begin{cases} C_m \cos(\alpha_m d/2) \exp[-\gamma_m (x - d/2)] & \text{if } x > d/2 \\ C_m \cos(\alpha_m x) & \text{if } -d/2 |x| \leq d/2 \\ C_m \cos(\alpha_m d/2) \exp[\gamma_m (x + d/2)] & \text{if } x < -d/2 \end{cases} \tag{5.15}$$

for $m = 0, 2, 4, \ldots$ (symmetric modes) and

$$X_m(x) = \begin{cases} S_m \sin(\alpha_m d/2) \exp[-\gamma_m (x - d/2)] & \text{if } x > d/2 \\ S_m \sin(\alpha_m x) & \text{if } |x| \leq d/2 \\ -S_m \sin(\alpha_m d/2) \exp[\gamma_m (x + d/2)] & \text{if } x < -d/2 \end{cases} \tag{5.16}$$

for $m = 1, 3, 5, \ldots$ (antisymmetric modes), with

$$\begin{aligned} \alpha_m &= \left(k_0^2 n_\mathrm{g}^2 - \beta_m^2\right)^{1/2}, \\ \gamma_m &= \left(\beta_m^2 - k_0^2 n_\mathrm{c}^2\right)^{1/2}. \end{aligned} \tag{5.17}$$

The propagation constants can be solved from equation

$$\tan\left(\alpha_m d/2 - m\pi/2\right) = \frac{\gamma_m}{\alpha_m} \tag{5.18}$$

and the normalization constants are

$$C_m = \left[\frac{d}{2} + \frac{\sin\left(\alpha_m d\right)}{2\alpha_m} + \frac{\cos^2\left(\alpha_m d/2\right)}{\gamma_m}\right]^{-1/2}, \tag{5.19}$$

$$S_m = \left[\frac{d}{2} - \frac{\sin\left(\alpha_m d\right)}{2\alpha_m} + \frac{\sin^2\left(\alpha_m d/2\right)}{\gamma_m}\right]^{-1/2}. \tag{5.20}$$

In our numerical modeling we assume that the incident beam is of GSM form, but let it be shifted, tilted, or defocused with respect

to the front end of the wave guide. Therefore the modal fields including these alignment errors may be expressed as

$$\begin{aligned} v_n(x,z) = &\left(\frac{2}{\pi w_0^2 \beta}\right)^{1/4} \frac{1}{\sqrt{2^n n!}} \sqrt{\frac{w_0}{w(z)}} \exp\left[\mathrm{i}\psi(z)/2\right] \\ &\times H_n\left[\frac{\sqrt{2}}{w(z)\sqrt{\beta}}\left(x - x_0 - \theta_0 \Delta z\right)\right] \\ &\times \exp\left[-\frac{\left(x - x_0 - \theta_0 \Delta z\right)^2}{w^2(z)\beta}\right] \exp\left[\frac{\mathrm{i}k_0}{2R(z)}\left(x - x_0 - \theta_0 \Delta z\right)^2\right] \\ &\times \exp\left[\mathrm{i}k_0 \theta_0 \left(x - x_0 - \theta_0 \Delta z\right)\right] \end{aligned} \tag{5.21}$$

with $\psi(z) = k_0 \Delta z - \arctan\left(\Delta z / z_\mathrm{R}\right)$. The parameters x_0, θ_0, and Δz, represent the amount of lateral shift, angular tilt, and longitudinal defocus, respectively. The weights of the modes are

$$c_n = S_0 \sqrt{2\pi} w_0 \frac{\beta}{1+\beta} \left(\frac{1-\beta}{1+\beta}\right)^n. \tag{5.22}$$

The other parameters are of the usual form for the coherent modes Hermite–Gaussian beams: denoting the Rayleigh range by $z_\mathrm{R} = \pi w_0^2 / \lambda$ and defining $\beta = \left[1 + \left(w_0/\sigma_0\right)\right]^{-1/2}$,

$$w(z) = w_0 \left(1 + \frac{\Delta z^2}{z_\mathrm{R}^2}\right)^{1/2} \tag{5.23}$$

is the beam width at position z,

$$\sigma(z) = \frac{\sigma_0}{w_0} w(z), \tag{5.24}$$

is the rms coherence width, and

$$R(z) = \Delta z + \frac{z_\mathrm{R}^2}{\Delta z} \tag{5.25}$$

is the radius of curvature of the wave front.

Figure 5.3 provides one example of coupling of an imperfectly aligned incident beam into the waveguide. Here the parameters are

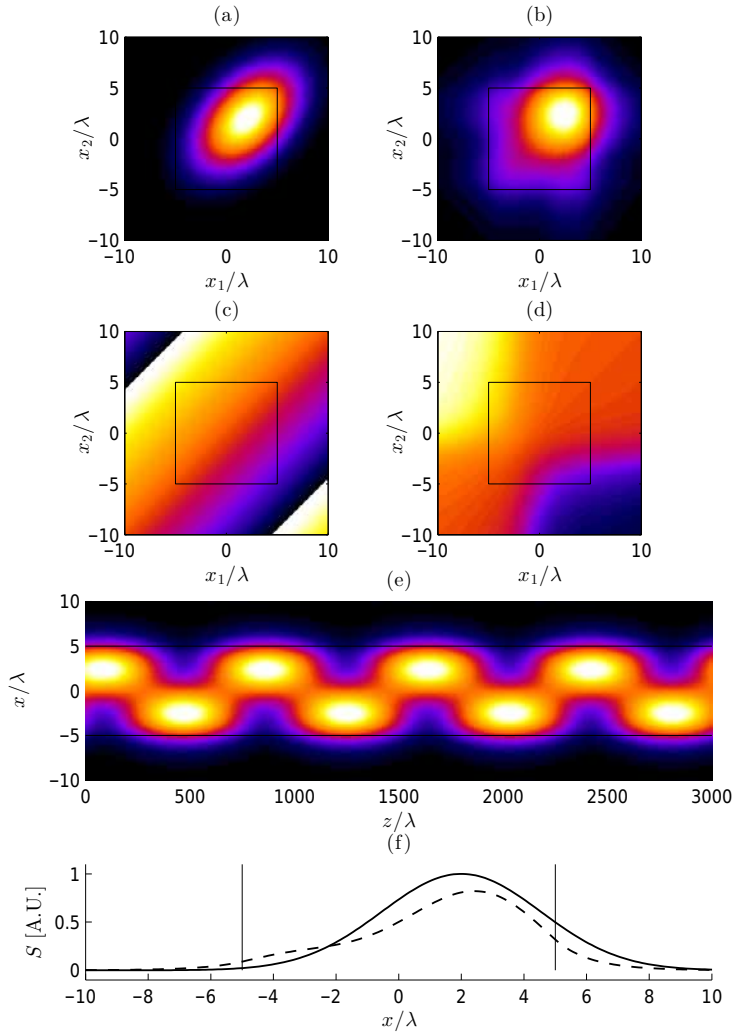

Figure 5.3: Coupling of a GSM beam into a waveguide. (a) The absolute value of the incident CSD. (b) The absolute value of the guided CSD. (c) The phase of the incident CSD. (b) The phase value of the guided CSD. (e) Intensity profile of the guided field inside the waveguide. (f) Comparison of the intensities of the incident and guided fields at $z = 0$.

$w_0 = 5.09\lambda_0$, $\sigma_0 = 4\lambda_0$, $d = 10\lambda_0$, $n_\mathrm{g} = 1.503$, $n_\mathrm{c} = 1.500$, $x_0 = 2\lambda$, $\theta_0 = 2°$, and $\Delta z = 0\lambda_0$. This waveguide supports two propagating modes. In Fig. 5.3(a) we show the absolute value of CSD of the

input beam right before the interface and 5.3(b) illustrates the CSD of the coupled beam right after the interface. In 5.3(c) and (d) we show the corresponding phases. Propagation of the field inside the waveguide is illustrated in 5.3(e), from which we see how the intensity alternates periodically, repeating itself after interval of 800 wavelengths. Therefore we may call the guided field self imaging. Finally, in 5.3(c) we compare the input and coupled intensities. The boxes and lines in the figures represent the edges of the waveguide, $x = \pm d/2$.

More results with different parameters are shown in the Paper **IV**. Waveguides with similar structure have also been studied in THz [98] and X-ray [99, 100] regimes.

5.4 SUMMARY

In this Chapter we propagated partially coherent beams in free space using measured coherence data. While this method is very accurate, the measurement to acquire the required data may take too long for routine use. Fortunately the elementary-field method was seen to often provide sufficiently accurate results with very simple measurements. We also considered the application of the coherent mode decomposition of partially coherent light to propagation in optical systems. In particular, coupling of light into planar waveguide was considered as an example.

6 Discussion and conclusions

In this thesis we summarized the basic concepts of spatial coherence of scalar fields together with two types of modal representations, described the Gaussian Schell model (GSM) as a useful approximation of many partially coherent fields, and studied briefly numerical sampling issues with the aid of the GSM fields. Then we introduced some coherence measurement systems and concentrated on the broad area laser diode as our real example source. Finally, a theoretical model for coupling partially coherent light into planar waveguides was presented.

Some of the work reported in this thesis is of theoretical nature (in particular Paper **IV**) with numerical simulation on propagation of partially coherent fields. Much of the emphasis, however, has been on experimental characterization of spatially partially coherent fields generated by real sources (such as BALDs) and field obtained by interferometric conversion of conventional partially coherent fields. Experimental verification of many interesting phenomena in optical coherence theory is still missing, perhaps because most members of the optical coherence research community are theoretically oriented. The results presented here and in the associated Papers **I–III** should therefore be a welcome addition to the existing literature.

Our realization of the classical Young's interferometer with a digital micromirror device (DMD) is novel technological approach to spatial coherence measurement. The device is capable of detecting both the absolute value and the phase of the cross spectral density, allowing numerical construction of the coherent-mode representation of a partially coherent field from experimental results at a higher resolution than ever before (to our knowledge). As a result, even the small details of the BALD were resolved, and theoretical models based on these results agreed with direct measurements of the propagated beam surprisingly well. With some further de-

velopment, our prototype could have many applications in science and industry, for example when the behavior of a high power laser beam in optical systems need to be modeled. With a more sensitive camera and a more polished control software, the speed of the system could be increased further.

Even with the DMD setup, the measurement of the CSD at high resolution takes hours. However, it was demonstrated that relatively simple intensity measurement systems without special components can be useful for characterization of the coherence properties of real light sources and beams radiated by them. When the elementary-field method is used, it is enough to simply measure the intensity profiles at the source plane and in the far zone to determine the shape of the elementary modes and their weight function, and subsequently simulate the field propagation numerically at an accuracy that is sufficient for most practical applications.

In most of this thesis we only considered y invariant sources and fields, measuring and calculating the coherence functions only in the x direction. This was well justified for BALDs, which are essentially coherent in the y direction. However, many other light sources can at least be approximated as being separable in x and y directions, and therefore it is enough to measure the CSD separately these directions, yielding $W(x_1, x_2)$ and $W(y_1, y_2)$ that can be multiplied to form the entire CSD. If the source is more complicated and CSD is inseparable, a four-dimensional CSD $W(x_1, x_2, y_1, y_2)$ is required. The measurement time would then increase beyond any practical limit even with our reasonably fast measurement set up, at least if high-resolution such as those presented in this thesis are required. Therefore, in the future, it is important to consider suitable sampling criteria for different kind of lights sources, so that we do not waste time measuring unnecessary information to model the spatial coherence properties of light. The author has already carried out some simulations to this end, which however were not presented above and may lead to a publication.

We also assumed throughout the thesis that the sources are linearly polarized and can therefore be described by the scalar the-

ory of light (at least in the paraxial domain). Many realistic light sources are, however, either partially polarized or essentially unpolarized. To handel beamlike sources (and fields) we need to expand the analysis to the domain of electromagnetic optics. In the case of highly directional (beamlike) fields, the scalar CSD used here must be replaced by a 2×2 CSD tensor. If the angular spread of the radiated beam extends to the non-paraxial domain, the CSD tensor that should consider is a 3×3 tensor, which also takes into account the z component of the electric field.

Experimental characterization of full vectorial CSD tensors is not easy, but the diagonal components of the tensor may at least in some cases be measured by placing a rotatable polarizer in front of the beam. The off-diagonal components are more difficult to treat and would require at least polarization modifications on the Young's measurement pinholes separately. This in turn would probably require a customized array of controllable micro polarizers. Also we would have to detect the interference fringes in terms of the degree of polarization instead of an easily detectable intensity as we now did in traditional Young's experiment. The author envisages that a lot of effort will be needed to resolve this kind of question, at both theoretical and experimental levels.

We demonstrated how coherence properties of light can be modulated using simple wavefront folding interferometer. We also described how the time-averaged degree of coherence may be decreased using a simple rotating diffuser. Modifications of state of coherence can be important for example when trying to get rid off speckle pattern in laser illumination systems. However, also these studies were restricted to the domain of scalar optics. Interesting new polarization-dependent phenomena might be revealed by illuminating the interferometer with vectorial fields having a space-variant polarization state.

Finally we presented a theoretical approach for coupling partially coherent beams into planar waveguides, considering only TE polarization. Further work is needed to characterize other waveguides, such as planar waveguides of more complicated form than

the single-layer guide considered here, optical fibers (including microstructured and photonic-crystal fibers), and two-dimensional channel waveguides. In two-dimensional geometries the electromagnetic nature of light would again have to be considered.

As a final remark, it has become clear to the author that not all questions that arise during one's Ph.D. work can be answered during the limited time period allowed for the completion of the thesis.

Bibliography

[1] L. Mandel and E. Wolf, *Optical Coherence and Quantum Optics* (Cambridge University Press, Cambridge, 1995).

[2] E. Wolf, *Introduction to the Theory of Coherence and Polarization of Light* (Cambridge University Press, 2007).

[3] M. J. Beran and G. B. Parrent, *Theory of Partial Coherence* (Prentice-Hall, 1964).

[4] J. W. Goodman, "Some fundamental properties of speckle," *J. Opt. Soc. Am.* **66,** 1145–1150 (1976).

[5] N. George and A. Jain, "Speckle Reduction Using Multiple Tones of Illumination," *Appl. opt.* **12,** 1202–1212 (1973).

[6] T. Young, "The Bakerian Lecture: On the Theory of Light and Colours," *Philosophical Transactions of the Royal Society of London* **92,** 1248 (1802).

[7] T. Young, "The Bakerian Lecture: Experiments and Calculations Relative to Physical Optics," *Philosophical Transactions of the Royal Society of London* **94,** 116 (1804).

[8] A. J. Fresnel, *Œuvres complètes d'Augustin Fresnel: Théorie de la lumière* (Imprimerie impériale, 1866).

[9] F. Zernike, "The concept of degree of coherence and its applications to optical problems," *Physica* **5,** 785–795 (1938).

[10] F. Gori and M. Santarsiero, "Devising genuine spatial correlation functions," *Opt. Lett* **32,** 3531–3533 (2007).

[11] F. Gori, V. Ramírez-Sánchez, M. Santarsiero, and T. Shirai, "On genuine cross-spectral density matrices," *J. Opt. A: Pure Appl. Opt.* **11,** 3531–3533 (2009).

[12] J. Tervo, T. Setälä, and A. T. Friberg, "Theory of partially coherent electromagnetic fields in the space-frequency domain," *J. Opt. Soc. Am. A* **21,** 2205–2215 (2004).

[13] E. Wolf, "New theory of partial coherence in the space-frequency domain. Part I: spectra and cross spectra of steady-state sources," *J. Opt. Soc. Am.* **72,** 343–351 (1982).

[14] MathWorks, "Eigenvalues and eigenvectors - MATLAB eig," `http://se.mathworks.com/help/matlab/ref/eig.html` (2015), [valid; 11-November-2015].

[15] A. C. Schell, "A technique for the determination of the radiation pattern of a partially coherent source," *IEEE Trans. Antennas Propag.* **AP-15,** 187–188 (1967).

[16] F. Gori and C. Palma, "Partially coherent sources which give rise to highly directional fields," *Opt. Commun.* **27,** 185–187 (1978).

[17] F. Gori, "Directionality and partial coherence," *Opt. Acta.* **27,** 1025–1034 (1980).

[18] P. Vahimaa and J. Turunen, "Finite-elementary-source model for partially coherent radiation," *Opt. Express* **14,** 1376–1381 (2006).

[19] J. Turunen and P. Vahimaa, "Independent-elementary-field model for three-dimensional spatially partially coherent sources," *Opt. Express* **16,** 6433–6442 (2008).

[20] P. Vahimaa and J. Turunen, "Independent-elementary-pulse representation for non-stationary fields," *Opt. Express* **14,** 5007–5012 (2006).

[21] J. Tervo, J. Turunen, P. Vahimaa, and F. Wyrowski, "Shifted-elementary-mode representation for partially coherent vectorial fields," *J. Opt. Soc. Am. A* **27,** 2004–2014 (2010).

[22] J. Turunen, "Elementary-field representations in partially coherent optics," *J. Mod. Opt.* **58,** 509–527 (2011).

[23] H. Hyvärinen, J. Turunen, and P. Vahimaa, "Elementary-field modeling of surface-plasmon excitation with partially coherent light," *Appl. Phys. B* **101,** 283–282 (2010).

[24] M. Singh, J. Tervo, and J. Turunen, "Elementary-field analysis of partially coherent beam shaping," *J. Opt. Soc. Am. A* **30,** 2611–2617 (2013).

[25] M. Singh, J. Tervo, and J. Turunen, "Broadband beam shaping with harmonic diffractive optics," *Opt. Express* **22,** 22680–22688 (2014).

[26] M. Singh, H. Lajunen, J. Tervo, and J. Turunen, "Imaging with partially coherent light: elementary-field approach," *Opt. Express* **23,** 28132–28140 (2015).

[27] S. Kawata, I. Hikima, Y. Ichihara, and S. Watanabe, "Spatial coherence of KrF excimer lasers," *Appl. Opt.* **31,** 387–396 (1992).

[28] Z. Huang and K.-J. Kim, "Review of x-ray free-electron laser theory," *Phys. Rev. ST AB* **10,** 034801 (2007).

[29] S. Roling, B. Siemer, M. Wöstmann, H. Zacharias, R. Mitzner, A. Singer, K. Tiedtke, and I. A. Vartanyants, "Temporal and spatial coherence properties of free-electron-laser pulses in the extreme ultraviolet regime," *Phys. Rev. ST AB* **14,** 080701 (2011).

[30] A. T. Friberg and R. J. Sudol, "Propagation parameters of gaussian Schell-model beams," *Optics Commun.* 383-387 (1982).

[31] P. W. Milonni and J. H. Eberly, *Laser Physics* (Wiley, New York, 2010).

[32] A. Siegman, "New developments in laser resonators," Proc. SPIE 1224, 2 (1990).

[33] F. Gori, "ColletWolf sources and multimode lasers," *Opt. Commun.* **32,** 301–305 (1980).

[34] A. Starikov and E. Wolf, "Coherent-mode representation of Gaussian Schell-model sources and of their radiation fields," *J. Opt. Soc. Am.* **72,** 923–928 (1982).

[35] Y. Li and E. Wolf, "Radiation from anisotropic Gaussian Schell-model sources," *Opt. Lett.* **7,** 256–258 (1982).

[36] P. DeSantis, F. Gori, G. Guattari, and C. Palma, "Anisotropic Gaussian Schell-model sources," *Opt. Acta* **33,** 315–326 (1986).

[37] J. Turunen, "Low Coherence Laser Beams," in *Laser Beam Propagation: Generation and Propagation of Customized Light*, A. Forbes, ed. (CRC Press, Boca Raton, 2014).

[38] A. Starikov, "Effective number of degrees of freedom of partially coherent sources," *J. Opt. Soc. Am* **72,** 1538–1544 (1982).

[39] R. Mitzner, M. N. B. Siemer1, T. Noll, F. Siewert, S. Roling, M. Rutkowski, A. Sorokin, M. Richter, P. Juranic, K. Tiedtke, W. E. J. Feldhaus and, , and H. Zacharias1, "Spatio-temporal coherence of free electron laser pulses in the soft X-ray regime," *Opt. Express* **16,** 19909–19919 (2008).

[40] T. Gensty, K. Becker, I. Fischer, W. Elsäßer, C. Degen, P. Debernardi, and G. P. Bava, "Wave chaos in real-world vertical-cavity surface-emitting laser," *Phys. Rev. Lett.* **94,** 233901 (2005).

[41] A. Valle and L. Pesquera, "Analytical calculation of transverse-mode characteristics in vertical-cavity surface-emitting lasers," *J. Opt. Soc. Am. B* **19,** 1549–1557 (2002).

[42] M. Peeters, G. Verschaffelt, H. Thienpont, S. K. Mandre, I. Fischer, and M. Grabherr, "Spatial decoherence of pulsed broad-area vertical-cavity surface-emitting lasers," *Opt. Express* **13** (2005).

[43] H.-J. Yoo, J. R. Hayes, E. G. Paek, A. Scherer, and Y.-S. Kwon., "Array mode analysis of two-dimensional phased arrays of vertical-cavity surface-emitting lasers," *IEEE J. Quantum Electron.* **26,** 1039–1051 (1990).

[44] D. S. Wiersma, "The physics and applications of random lasers," *Nature Physics* **4,** 359–367 (2008).

[45] H. Cao, Y. G. Zhao, S. T. Ho, E. W. Seelig, Q. H. Wang, and R. P. H. Chang, "Random laser action in semiconductor powder.," *Phys. Rev. Lett.* **82,** 2278–2281 (1999).

[46] N. Stelmakh and M. Flowers, "Measurement of spatial modes of broad-area diode Lasers with 1-GHz resolution grating spectrometer," *IEEE Photon. Technol. Lett.* **18,** 1618–1620 (2006).

[47] N. Stelmakh, "Harnessing multimode broad-area daser-diode emission into a single-lobe diffraction-limited spot," *IEEE Photon. Technol. Lett.* **19,** 1392–1394 (2007).

[48] N. Stelmakh, "Combining of modes of broad-area laser diode into a single-mode spot," *Conference on Lasers and Electro-Optics, 2007. CLEO 2007* 1–2 (2007).

[49] J.-M. Verdiell and R. Frey, "A Broad-Area Mode-Coupling Model for Multiple-Stripe Semiconductor Lasers," *IEEE J. Quant. Electron.* **26,** 270–279 (1990).

[50] C. Liu, J. Ge, and J. Chen, "Study on a broad-area laser diode with external cavity feedback," *Optics & Laser Technology* **39,** 169173 (2005).

[51] D. F. Welch, "A brief history of high-power semiconductor lasers," *IEEE J. Sel Top. Quant.* **6,** 1470–1477 (2000).

[52] H. Zappe, *Laser Diode Microsystems* (Springer, Berlin, 2003).

[53] I. Fischer, O. Hess, W. Elsäßer, and E. Göbel, "Complex spatio-temporal dynamics in the near-field of a broad-area semiconductor laser," *Europhys. Lett.* **35,** 579–584 (1996).

[54] M. O. Ziegler, M. Münkel, T. Burkharda, G. Jennemanna, I. Fischer, and W. Elsässer, "Spatiotemporal emission dynamics of ridge waveguide laser diodes: picosecond pulsing and switching," *J. Opt. Soc. Am. B* **16,** 2015–2022 (1999).

[55] T. Burkharda, M. O. Ziegler, I. Fischer, and W. Elsäßer, "Spatio-temporal Dynamics of Broad Area Semiconductor Lasers and its Characterization," *Chaos, Solitons & Fractals* **10,** 845–850 (1999).

[56] J. Turunen, E. Tervonen, and A. T. Friberg, "Coherencetheoretic algorithm to determine the transverse mode structure of lasers," *Opt. Lett.* **14,** 627–629 (1989).

[57] F. Gori, M. Santarsiero, R. Borghi, and G. Guattari, "Intensity-based modal analysis for partially coherent beams with Hermite-Gaussian modes," *Opt. Lett.* **23,** 989–991 (1998).

[58] M. Santarsiero, F. Gori, R. Borghi, and G. Guattari, "Evaluation of the modal structure for light beams made by incoherent mixtures of Hermite-Gaussian modes," *Appl. Opt.* **38,** 5272–5281 (1999).

[59] R. Borghi, G. Piquero, and M. Santarsiero, "Use of biorthogonal functions for the modal decomposition of multimode beams," *Opt. Commun.* **194,** 235–242 (2001).

[60] R. Borghi, G. Guattari, L. de la Torre, F. Gori, and M. Santarsiero, "Evaluation of the spatial coherence of a light beam through transverse intensity measurements," *J. Opt. Soc. Am. A* **20,** 1763–1770 (2003).

[61] H. Partanen, *Puolijohdevalolähteiden moodeja* (University of Eastern Finland, 2011).

[62] "Theme issue, Interference: 200 years after Thomas Young's discoveries," *Philosophical Transactions of the Royal Society of London* **360,** 805–1069 (2002).

[63] B. E. A. Saleh and M. C. Teich, *Fundamentals of Photonics* (Wiley, New York, 2007).

[64] E. Tervonen, J. Turunen, and A. T. Friberg, "Transverse laser-mode structure determination from spatial coherence measurements: Experimental results," *Appl. Phys. B* **49,** 409–414 (1989).

[65] B. Anderson and P. Fuhr, "Twin-fiber interferometric method for measuring spatial coherence," *Opt. Eng.* **32,** 926–932 (1993).

[66] C. K. Hitzenberger, M. Danner, W. Drexler, and A. F. Fercher, "Measurement of the spatial coherence of superluminescent diodes," *J. Mod. Opt.* **46,** 1763–1774 (1999).

[67] C. M. Warnky, B. L. Anderson, and C. A. Klein, "Determining spatial modes of lasers with spatial coherence measurements," *Appl. Opt.* **39,** 6109–6117 (2000).

[68] M. Santarsiero and R. Borghi, "Measuring spatial coherence by using a reversed-wavefront Young interferometer," *Opt. Lett.* **31,** 861–863 (2006).

[69] Y. Mejia and A. Gonzalez, "Measuring spatial coherence by using a mask with multiple apertures," *Opt. Commun.* **273,** 428–434 (2007).

[70] K. Saastamoinen, J. Tervo, J. Turunen, P. Vahimaa, and A. T. Friberg, "Spatial coherence measurement of polychromatic light with modified Young's interferometer," *Opt. Express* **21,** 4061–4071 (2012).

[71] D. Dudley, W. M. Duncan, and J. Slaughter, "Emerging digital micromirror device (DMD) applications," *Proc. SPIE* **4985,** 14–25 (2003).

[72] Y.-X. Ren, R.-D. Lu, , and L. Gong, "Tailoring light with a digital micromirror device," *Annalen der Physik* **527,** 447–470 (2015).

[73] N. A. Riza, S. A. Reza, and P. J. Marraccini, "Digital Micromirror Device-based broadband optical image sensor for robust imaging applications," *Optics Commun.* **284,** 103–111 (2011).

[74] Y.-X. Ren, Z.-X. Fang, L. Gong, K. Huang, Y. Chen, and R.-D. Lu, "Digital generation and control of Hermite-Gaussian modes with an amplitude digital micromirror device," *Journal of Optics* **17,** 125604 (2015).

[75] M. Sheikh and N. A. Riza, "Demonstration of Pinhole Laser Beam Profiling Using a Digital Micromirror Device," *IEEE Photonic. Tech. L.* **21,** 666–669 (2009).

[76] M. Sheikh and N. A. Riza, "Motion-free hybrid design laser beam propagation analyzer using a digital micromirror device and a variable focus liquid lens," *Appl. Opt.* **49,** D6–11 (2010).

[77] H. Partanen, S. Peterhaensel, C. Pruss, W. Osten, J. Tervo, and J. Turunen, "Broad area laser diode coherence measurement and modeling," *Fringe 2013* 879–882 (2014).

[78] J. Lehtolahti, M. Kuittinen, J. Turunen, and J. Tervo, "Coherence modulation by deterministic rotating diffusers," *Opt. Express* **23,** 10453–10466 (2015).

[79] Y. Q. G. Li and H. Li, "Coherence theory of a laser beam passing through a moving diffuser," *Opt. Express* **21,** 13032–13039 (2013).

[80] Q. He, J. Turunen, and A. T. Friberg, "Propagation and imaging experiments with Gausian Schell-model beams," *Opt. Commun.* **67,** 245–250 (1988).

[81] H. W. Wessely and J. O. Bolstadt, "Interferometric technique for measuring the spatial-correlation function of optical radiation fields," *J. Opt. Soc. Am.* **60,** 678–682 (1970).

[82] J. B. Breckinridge, "Coherence interferometer and astronomical applications," *Appl. Opt.* **11,** 2996–2998 (1972).

[83] G. Verschaffelt, G. Craggs, M. L. F. Peeters, S. K. Mandre, H. Thienpont, and I. Fischer, "Spatially resolved characterization of the coherence area in the incoherent emission regime of a broad-area vertical-cavity surface-emitting laser," *IEEE J. Quant. Electron.* **45,** 249–255 (2009).

[84] H. Arimoto and Y. Ohtsuka, "Measurements of the complex degree of spectral coherence by use of a wave-front-folded interferometer," *Opt. Lett.* **22,** 958–960 (1997).

[85] J. H. McLeod, "The Axicon: A New Type of Optical Element," *J. Opt. Soc. Am.* **44,** 592–597 (1954).

[86] F. Gori and G. Guattari, "Modal expansion for J_0-correlated Schell-model sources," *Opt. Commun.* **64,** 311316 (1987).

[87] S. Y. Popov and A. T. Friberg, "Linear axicons in partially coherent light," *Opt. Eng.* **34,** 2567–2573 (1995).

[88] A. T. Friberg and S. Y. Popov, "Radiometric description of intensity and coherence in generalized holographic axicon images," *Appl. opt.* **35,** 3039–3046 (1996).

[89] F. Gori, G. Guattari, C. Palma, and C. Padovani, "Specular cross-spectral density functions," *Opt. Commun.* **68,** 239–243 (1988).

[90] M. Mansuripur, "Certain computational aspects of vector diffraction problems," *J. Opt. Soc. Am. A* **6,** 786–805 (1989).

[91] K. Matsushima and T. Shimobaba, "Band-Limited Angular Spectrum Method for Numerical Simulation of Free-Space

Propagation in Far and Near Fields," *Opt. Express* **17,** 19662–19673 (2009).

[92] X. Yu, T. Xiahui, Q. Yingxiong, P. Hao, and W. Wei, "Band-limited angular spectrum numerical propagation method with selective scaling of observation window size and sample number," *J. Opt. Soc. Am. A* **29,** 2415–2420 (2012).

[93] P. Spano, "Connection between spatial coherence and modal structure in optical fibers and semiconductor lasers," *Opt. Commun.* **33,** 265–270 (1980).

[94] S. Piazzolla and S. D. Marchis, "Spatial coherence in optical fibers," *Opt. Commun* **32,** 380–382 (1980).

[95] M. Imai, K. Itoh, and Y. Ohtsuka, "Measurements of complex degree of spatial coherence at the end face of an optical fiber," *Opt. Commun.* **42,** 97–100 (1982).

[96] S. Piazzolla and P. Spano, "Spatial coherence in incoherently excited optical fibers," *Opt. Commun.* **43,** 175–179 (1982).

[97] T. Saastamoinen, M. Kuittinen, P. Vahimaa, J. Turunen, and J. Tervo, "Focusing of partially coherent light into planar waveguides," *Opt. Express* **12,** 4511–4522 (2004).

[98] S. Withington and G. Yassin, "Analyzing the power coupled between partially coherent waveguide fields in different states of coherence," *J. Opt. Soc. Am. A* **19,** 1376–1382 (2002).

[99] K. J. Tsanaktsidis, D. M. Paganin, and D. Pelliccia, "Analytical description of partially coherent propagation and absorption losses in x-ray planar waveguides," *Opt. Lett.* **38,** 1808–1810 (2013).

[100] M. Osterhoff and T. Salditt, "Coherence filtering of x-ray waveguides: analytical and numerical approach," *New J. Phys.* **13,** 103026 (2011).

Henri Partanen

Modeling and measurement of partial spatial coherence

This thesis considers methods to measure and model the coherence function of the light sources. Young's interferometer realized with digital micromirror devices is introduced and the data is used to accurately simulate the behavior of the beams. Broad area laser diode is used as an example of a clearly partially coherent source with complicated modal structure. Methods to modify the coherence are considered. Finally coupling of the partially coherent beams into waveguides is analyzed.

UNIVERSITY OF
EASTERN FINLAND

Publications of the University of Eastern Finland
Dissertations in Forestry and Natural Sciences

ISBN: 978-952-61-1534-4 (printed)
ISSN: 1798-5668
ISBN: 978-952-61-1535-1 (pdf)
ISSN: 1798-5676